

AMERICAN UNIVERSITY OF BEIRUT

Measurement and Analysis of Low-Temperatures
Thermal Properties of Low-Dimensional
Materials

by

Hana Jamil Baroudi

A thesis

submitted in partial fulfillment of the requirements
for the degree of Master of Science
to the Department of Physics
of the Faculty of Arts and Sciences
at the American University of Beirut

Beirut, Lebanon

May 2018

AMERICAN UNIVERSITY OF BEIRUT

Measurement and Analysis of Low-Temperatures Thermal Properties of Low-Dimensional Materials

by

Hana Jamil Baroudi

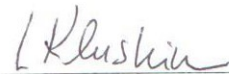
Approved by:



Dr. Michel Kazan, Associate Professor

Advisor

Physics



Dr. Leonid Klushin, Professor

Member of Committee

Physics



Dr. Malek Tabbal, Professor

Member of Committee

Physics

Date of thesis defense: May 8, 2018

AMERICAN UNIVERSITY OF BEIRUT

THESIS, DISSERTATION, PROJECT RELEASE FORM

Student Name: Boreudi Homa Jamil
Last First Middle

Master's Thesis Master's Project Doctoral Dissertation

I authorize the American University of Beirut to: (a) reproduce hard or electronic copies of my thesis, dissertation, or project; (b) include such copies in the archives and digital repositories of the University; and (c) make freely available such copies to third parties for research or educational purposes.

I authorize the American University of Beirut, to: (a) reproduce hard or electronic copies of it; (b) include such copies in the archives and digital repositories of the University; and (c) make freely available such copies to third parties for research or educational purposes after:
One ___ year from the date of submission of my thesis, dissertation or project.
Two ___ years from the date of submission of my thesis, dissertation or project.
Three ___ years from the date of submission of my thesis, dissertation or project.

Homa Boreudi May 14, 2018
Signature Date

This form is signed when submitting the thesis, dissertation, or project to the University Libraries

Acknowledgements

Firstly, i would like to express my sincere gratitude to my advisor Prof. Michel Kazan for his continuous support in my Master's study and related research. This work wouldn't have been possible without his patience, motivation and immense knowledge. His guidance has helped me throughout all the hardships and difficulties of my studies. I could not have imagined having a better advisor and mentor for my Master's study.

Besides my advisor, i would like to thank my thesis committee members: Prof. Leonid Klushin and Prof. Malek Tabbal not only for their insightful comments and encouragement, but also for their difficult questions which incited me to widen my research from various perspectives. A special thanks for Prof. Klushin's remarks that have helped me shift my work in the proper direction.

My sincere thanks to Dr. Abdo Iskandar who has provided me with the opportunity to accompany him in the laboratory and to learn from his extensive knowledge.

Last but not least, i thank my fellow colleagues and friends for the stimulating discussions, the sleepless nights and their continuous support and motivation.

An Abstract of the Thesis of

Hana Jamil Baroudi for Master of Science

Major: Physics

Title: Measurement and Analysis of Low-Temperatures Thermal Properties of Low-Dimensional Materials

In this work, we report calorimetric measurements of the specific heat of Zinc Oxide nanowires and graphene. We also determine the thermal conductance of the interface between the vertically aligned Zinc Oxide nanowires and Silicon substrate. Heat-pulse calorimetric technique was applied to free-surface Zinc Oxide nanowires and clamped graphene samples. The temperature response of the heat-pulse calorimeter was analyzed by a model that takes into account the effect of the thermal conductance between the nanowires and the substrate. The specific heat of the samples and the thermal conductance of the interface were determined from 1.8 to 300 K using a linear least squares method. It is found that the low temperatures behavior (below 4 K) of the Zinc Oxide nanowires' specific heat admits a two-dimensional crystal contribution in addition to the bulk T^3 dependence. Above 25 K, The specific heat of the nanowires is enhanced compared to that of the bulk Zinc Oxide and this enhancement increases as the

temperature increases and the nanowires diameter decreases. As for the thermal conductance of the interface between the Silicon substrate and Zinc Oxide nanowires, it is found to be orders of magnitude lower than that between bulk ZnO and Si substrate, suggesting the formation of thin layer of low crystallinity between the nanowires and Silicon substrate. Furthermore, the recorded data demonstrated transition from specular to diffusive elastic transmission, and then from diffusive elastic to diffusive inelastic transmission as temperature increases. Also, the specific heat of clamped graphene at low-temperatures was found to follow a two-dimensional behavior confirming the T^2 dependence theories reported in the theoretical models. This specific heat of graphene shows an increase in its values at higher temperatures in comparison with graphite.

Contents

Acknowledgements	v
Abstract	vi
1 Introduction	1
2 Theoretical study	8
2.1 Basic concepts and definitions	8
2.2 Lattice Specific heat Models	10
2.2.1 The Dulong and Petit Law	10
2.2.2 The Einstein Model	11
2.2.3 The Debye Model	13
2.3 Specific Heat Measurement Techniques at Low-temperatures . . .	16
2.4 Nanowires specific heat Model	18
2.4.1 Dispersion Relation	19
2.4.2 Density of states	21
2.4.3 Specific Heat	24
2.5 Clamped Graphene specific heat Model	25
2.5.1 Dispersion Relation	26
2.5.2 Density of states	27

2.5.3	Specific Heat	29
3	Experimental Study	30
3.1	Analysis Methods	31
3.1.1	One-Tau Model	31
3.1.2	Two-Tau Model	34
3.1.3	Three-Tau Model	35
3.2	Experimental Setup	36
3.2.1	Nanowires Sample Synthesis	37
3.2.2	Nanowires Sample Characterization	38
3.2.3	Calorimetric Measurement	40
4	Results and Discussion	44
4.1	Specific heat Measurement	44
4.1.1	Addenda Measurement	44
4.1.2	Substrate Measurement	45
4.1.3	ZnO nanowires measurements	46
4.1.4	Graphene Measurement	51
4.2	Thermal Conductance between Si substrate and ZnO nanowires	54
5	Conclusion	57
A	Three-tau model derivation	59

List of Figures

1.1	a) nanowire array embedded in a matrix. b) free-surface nanowire array [1].	4
2.1	Scheme of the main elements of a calorimeter for measurements of heat capacity [2]	17
3.1	Heat flow diagram for the one tau simple model cases.	32
3.2	Heat pulse calorimetry principle. Heat is applied till $t = t_0$, after which the temperature starts to relax exponentially	33
3.3	Heat flow diagram for the two-tau model.	34
3.4	Heat flow diagram for the three-tau model	36
3.5	ZnO nanowires synthesis setup	38
3.6	Scanning electron microscopy image of the samples investigated	38
3.7	X-ray diffraction pattern of the samples investigated	39
3.8	Dynacool simplified schematic drawing. [3]	40
3.9	The puck 1792 (left) and the platform (right). 1: The sapphire platform 2: Au-Pd wires 3: Gold contacts 4: Thermometer 5: Heater. [4]	41

4.1	Heat capacity of the addenda and the empty puck; puck + 1mg of grease is shown in 'blue circles', puck+ 0.3mg of grease is shown in 'yellow square', empty puck is shown twice in 'red diamonds and green triangles'. [4]	45
4.2	Average specific heat of the Apiezon N grease (solid blue line) with its uncertainty (shaded area). The inset shows the low temperature behavior. [4]	46
4.3	Specific heat of the Silicon substrate alone (open symbols) and of the substrate with nanowires(colored symbols)	47
4.4	Specific heat of bulk ZnO obtained from first principles calculation (open symbols) and of the ZnO nanowires obtained from calorimetric measurements(colored symbols)	48
4.5	c/T versus T^2 for the Zinc Oxide bulk and nanowires. Open symbols correspond to data obtained from calorimetric measurements. Closed symbols correspond to data fitted with the model detailed in section 2.4	49
4.6	Specific heat of graphene reported from calorimetric measurements from 2.8 to 300 K	51
4.7	Specific heat of graphene reported from calorimetric measurements and experimental values of graphite adopted from [5]	52
4.8	C/T vs T plot corresponding to the investigated graphene sample. closed symbols: Data obtained from calorimetric measurements. Solid Lines: Data obtained from linear fitting.	53

4.9	Thermal conductance of the interface between the Silicon substrate and the bulk ZnO obtained from first principles calculation (filled symbols) and of that between the substrate and ZnO nanowires obtained from calorimetric measurements(open symbols)	55
-----	---	----

List of Tables

3.1	The structural characteristics of the ZnO nanowires in the measured samples.	42
4.1	Debye temperatures of the ZnO nanowires in the measured samples.	51

Chapter 1

Introduction

The everlasting dream of man to miniaturize his everyday devices is still an ongoing one. Although many achievements have been made in the synthesis of promising low-dimensional materials, the challenges that come with reducing the size and volume of structures are still many. One of the most significant issues that arise is heat dissipation control at low dimensions. Indeed, appropriate thermal management is essential for the success of low-dimensional devices. Indeed, the design and optimization of these devices requires a thorough knowledge of the laws that govern the thermal properties and heat transport mechanisms in low-dimensional materials. A great deal of effort, therefore, has been put into the study of the thermal properties of low-dimensional devices to obtain reliable data on these structures. Although significant work has been achieved in this field, some important issues still need to be addressed. In this work we look into the thermal properties of nanowires and graphene samples, the most recognized structures as candidates for next-generation electronic materials, that could overcome the critical bottleneck of heat dissipation of current high-tech devices [6].

While most research focuses on the electrical transport properties of nanowires, the thermal properties of these structures are attracting more and more interest. This can be understood by the unique properties they exhibit that makes them suitable candidate in technological applications [7]. The properties of nanowires rise mainly from two characteristics: First, the high length to diameter ratio which makes a nanowire a one-dimensional material with a large surface area compared to its volume. Second, quantum confinement effects which have observable consequences on the properties of nanowires when the phonon wavelengths become comparable to the physical dimensions of the nano-structures. This happens below a few degrees Kelvin and only in nanowires of diameters not exceeding 6 nm [8–10]. Nevertheless, the presence of free surfaces nanowires gives rise to distinct effects on their thermal properties even in the absence of phonon quantum effects [9, 11]. These features allow for the application of nanowires in many technological areas ranging from chemical and biological sensors, lasers, solar cells, and thermoelectric energy conversion devices [12–15].

Perhaps the most important thermal properties of a material is its specific heat, which closely relates to the electron and phonon behavior of the material [16]. Many experimental investigations have been conducted for the determination of the behavior of the specific heat of nanotubes and nanowires. The specific heat of single-walled carbon nanotubes grouped to form a rope is found to be larger than that of multi-walled nanotubes and graphite below 50 K with strong temperature dependence [17]. Multi-walled carbon nanotubes of few tens of nm in diameter were found to exhibit a linear specific heat at low temperatures, indicating a weak inter-wall coupling compared to graphite and a constant phonon density of states [18]. Also, it was shown that the multi-walled boron nitride nanotubes follow the same behavior as the multi-walled carbon nanotubes [19].

Further calorimetric studies have been carried out on titanium dioxide nanotubes to study their specific heat and phonon density of states [20]. It was shown that the anatase nanotubes' specific heat always exceeds that of bulk anatase. At low temperatures below 3 K, the specific heat curve is nearly constant, exceeding the bulk specific heat values by factors of 25 to 50 at about 1.5 K. This experimental observation was attributed to a transition from three-dimensional density of states to a lower-dimensional one as the average phonon wavelength becomes comparable to the nanotubes' wall thickness. From 5 K to 50 K the nanotubes specific heat follows a $T^{2.6}$ behavior instead of the T^3 dependence. At higher temperatures, from 60 K to 95 K, the specific heat of the anatase nanotubes is almost 20-30% higher than that of its bulk counterpart.

The specific heat of nanotubes was observed to be dependent on the morphology of the nanomaterials. This is attributed to the size and shape dependent phonon and surface density of states that determines the fundamental thermal properties of the measured nanoparticles [21]. Mizel et al. [17] have shown that multi-walled carbon nanotubes have a specific heat similar to that of graphite due to structural similarities between the two. The specific heat of multi-walled Boron nitride nanotubes was revealed to be approaching that of a two-dimensional sheet as the diameter of the nanotubes increases. [22]

As for nanowires, which are filled nanotubes, the different experimental techniques used to determine their specific heat can be categorized in two groups: one for the determination of single nanowires or nanowires embedded in a matrix [23, 24] and the other related to free-surface nanowires array measurement [25]. However, no strong conclusions can be drawn out of the experimental data because measurements were either performed at very high or very low temperatures limits [25], or on nanowires embedded in a matrix, which clamps their

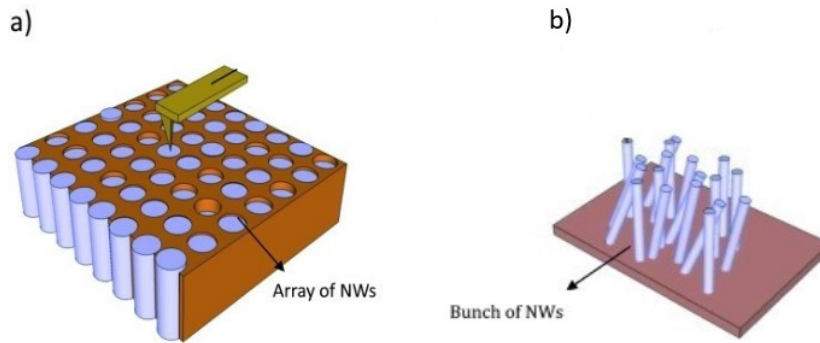


Figure 1.1: a) nanowire array embedded in a matrix. b) free-surface nanowire array [1].

surface and masks the looked-for contribution from the surface [8](see figure 1.1). Therefore, in this work we address this issue and offer a thorough experimental study of the specific heat of free-surface Zinc Oxide nanowires from 1.8 K to 300 K. We prove that the low temperatures specific heat behavior of the free-surface nanowires includes a two-dimensional contribution in addition to the bulk T^3 behavior. We also present an analytical model of the low-temperature specific heat of nanowires using continuum mechanics to confirm our results.

As for the study of thermal transport in low dimensional materials, numerous experiments have been conducted for the determination of the thermal conductivity of low-dimensional materials [26–33]. Many theories have been developed to explain these experimental results [34–38]. Single-wall and multi-wall carbon nanotubes have attracted a lot of attention due to the extraordinary thermal transport in one dimension. Ballistic and diffusive thermal transport modes and the breakdown of Fourier’s law have been observed in carbon nanotubes giving rise to their unique properties [39, 40]. In particular, semi-conductor nanowires have stood out as a potential candidate for applications in thermoelectric devices

due to their low thermal conductivity values compared to their bulk counterparts [28, 29]. The reason for this dramatic reduction in thermal conductivity of the nanowires is due to the enhanced phonon-boundary scattering with a reduction in sample size and possible phonon spectrum modification as a result of phonon confinement effects [27, 41]. Further theoretical investigations have been conducted for the purpose of studying the factors affecting the reduction of the thermal conductivity in order to reach a desirable thermoelectric figure of merit. These factors were found to be shape, size, length, purity, and surface asperities [41–48]. Moreover, it was found that vertically aligned nanowires grown on substrates have thermal conductivity values lower than that of individual nanowires [24, 49, 50], and consequently higher thermoelectric figure of merit [51, 52]. Also, the intermixing of the nanowires' atoms and silicon substrate atoms resulted in the amorphization of the surface underneath the wires which reduces the thermal conductivity of the wires [53]. However, the thermal resistance of the interface between the nanowires and the underlying substrate has never been measured. In this work, we address this issue and report calorimetric measurements of the thermal conductance of the interface between Silicon and Zinc Oxide nanowires from 1.8 to 300 K. we show that the thermal conductance between Si/ZnO nanowires is orders of magnitude lower than that of the interface between Si/ bulk-ZnO due to the formation of a thin layer of low crystallinity between the nanowires and the substrate. We also demonstrate the existence of different phonon transport regimes across the Si/ZnO nanowires interface as the excited phonon wavelengths change.

The other low dimensional material that has captivated the world's interest is graphene. This single layer of carbon atoms, is a two-dimensional material with exceptional optical [54, 55], electrical [56, 57], mechanical [58] and thermal

properties [59,60]. The uniqueness of graphene arises from its strong anisotropic sp^2 carbon bonds and the light weight of carbon atoms. Due to the quasi two-dimensional phonon transport and its ultra-high thermal conductivity, graphene is considered as the building block for many thermal management applications as heat spreaders in light emitting diodes, field-effect transistors, interconnects and fillers in thermal interface materials [61–66].

The phonon energy spectra are essential for the understanding of the phonon transport processes in graphene. Much theoretical [5,63,67–99] and experimental work [100–106] have been put into the description of phonons in single layer graphene, few-layers graphene and graphene nanoribbons. The theoretical models can be divided into three categories: (1) Lattice dynamics models [5,63,67–82], (2) elastic continuum mechanics models [83–89] and (3) ab-initio density functional theory computations [90–99]. As for the experimental investigations, they were carried out using inelastic x-ray scattering [100], inelastic electron tunneling spectroscopy [101] and Raman spectroscopy [102–106].

Though the work on graphene is abundant, it is still far from being sufficient. On one hand, the analytical and experimental data predicts different values for the thermal conductivity of graphene ranging from $600 \text{ W} \cdot (\text{m} \cdot \text{K})^{-1}$ to $5000 \text{ W} \cdot (\text{m} \cdot \text{K})^{-1}$ [107], and opposing dependence of the thermal conductivity on the thickness of graphene [108]. On the other hand, theoretical analysis of the specific heat of graphene at low temperatures, showed time dependence of T^n with n ranging from 1 to 1.1 [5,75,87]. However, up to this day no experimental measurements confirmed these results. It was also found that the specific heat of graphene is dependent on the supporting substrate [109], atomic rotation [5] and nanoribbon's width [110].

In this work, we report the experimental measurement of the low-temperatures

specific heat of single-layer clamped graphene sample by means of calorimetric measurement. The response of the graphene sample was measured directly with no supporting substrate and it was demonstrated that the low-temperatures behavior of the specific heat follows a two-dimensional behavior of T^2 as expected in theory.

Chapter 2

Theoretical study

In this chapter we present the theoretical aspects related to the specific heat of materials at low-temperatures. We review the basic models for the determination of the specific heat of bulk-materials and develop a theory for the calculation of the specific heat of nanowires at low-temperatures.

2.1 Basic concepts and definitions

The specific heat is a measure of the energy E needed to increase the temperature T of a body by one degree K, it is defined as:

$$c_x = \lim_{dT \rightarrow 0} \left(\frac{dE}{dT} \right)_x \quad (2.1)$$

where x represents the quantity that is fixed during measurement such as pressure or volume. The specific heat of a material depends on the temperature of the system and the way heat is transferred to the system. It is generally expressed in units of J/kg.K or J/mol.K. The most commonly used specific heats are determined at constant volume c_v and constant pressure c_p . The difference between

c_v and c_p referred to as the dilation contribution to the specific heat is expressed as:

$$c_p - c_v = \frac{V\beta^2}{\kappa_T}T \quad (2.2)$$

where $\beta = \frac{1}{V} \left(\frac{\partial V}{\partial T} \right)_P$ is the volume expansion coefficient and $\kappa_T = -\frac{1}{V} \left(\frac{\partial V}{\partial P} \right)_T$ is the isothermal compressibility, V the volume of the sample, T its temperature and P is the pressure acting on the sample. Since the latter is a positive quantity, c_p is always greater than c_v . However, when temperature goes to zero, the difference between the two specific heats tends to zero. This is seen by considering the third law of thermodynamics which states that as the temperature tends to zero the magnitude of the entropy, S , approaches a constant limiting value so that $\left(\frac{\partial S}{\partial P} \right)_T$ vanishes. Therefore, by the following Maxwell's relation $-\left(\frac{\partial V}{\partial T} \right)_P = \left(\frac{\partial S}{\partial P} \right)_T$, β goes to zero as the temperature tends to zero and hence c_p tends to c_v in the limit.

When conducting an experiment, we usually determine the specific heat at constant pressure since maintaining the volume of a solid constant requires very large pressures, which is a difficult task experimentally. However, at room temperature the difference between c_p and c_v rarely exceeds 4% and at low-temperatures (below 30 K) when the thermal expansion of solids is very small, the difference between the two specific heats is negligible [111]. For instance the ratio $\frac{c_p - c_v}{c_p}$ is found to be equal to 0.03% at $T=30\text{K}$ for Pd [112], and no difference between c_p and c_v is found for Al and Cu [113]. Therefore, we conclude that at low-temperatures c_p and c_v can be used interchangeably.

The heat carriers in any material are the electrons and phonons. The electrons contribute to the conduction process since they have non zero density of states

at the fermi energy. This adds a term to the the specific heat that is linear in temperature. However, the electronic states are only excited up to a few kelvins since transport by phonons dominates at higher temperatures. Therefore, the contribution of the electrons to the specific heat is neglected even at low temperatures. In this work, our focus will be on the analysis of the vibrational specific heat only at low temperatures.

2.2 Lattice Specific heat Models

In the following, different assumptions have been made for the determination of the energy of the phononic system in order to derive the specific heat of a material. We elaborate on the methods employed to determine the energy.

2.2.1 The Dulong and Petit Law

The transport of heat in a solid was envisaged by Boltzmann in 1896 [114] as a set of atoms vibrating around their lattice positions. Each atom interacts with its neighbors via a harmonic potential. So the atoms in a solid can be described as a set of masses connected by elastic springs in a simple harmonic motion. According to the principle of equipartition of energy, a linear harmonic oscillator has a mean internal energy of $k_B T$. The kinetic and potential energy contributing equally with a $\frac{1}{2}k_B T$. Hence the internal energy of a three-dimensional oscillator is equal to $3k_B T$. The average internal energy is thus:

$$E = 3Nk_B T = 3RT \tag{2.3}$$

where N is the number of atoms, k_B the boltzmann constant and R the ideal gas constant. The specific heat can thus be written as:

$$c_v = \frac{\partial E}{\partial T} = 3R \quad (2.4)$$

In the limit of this classical statistical mechanics picture, the specific heat of any material is a constant equal to $3R = 24.94 \text{ J/mol.K}$. This is the Dulong-Petit law predicted in 1819. After the discovery of cryogenic liquids, measurements were carried out and it was shown that the specific heat of all materials decreases rapidly with decreasing temperatures. For instance the specific heat of Cu is 24.43 J/mol.K at room temperature but it falls to a mere 0.0058 J/mol.K at 4K [115]. This drop in specific heat cannot be explained by classical theories, it had to wait for the development of quantum statistics.

2.2.2 The Einstein Model

To explain the dependence of the specific heat on temperature, Einstein [116] assumed that the atoms are simple harmonic oscillators that vibrate independently at the same frequency ω_E . The frequency distribution would thus be a delta function, for N oscillators $D(\omega) = 3N\delta(\omega - \omega_E)$. The average energy of a harmonic oscillator in each polarized direction is defined quantumly as $(\langle n \rangle + \frac{1}{2})\hbar\omega$ with $\langle n \rangle$ being the Bose-Einstein distribution $\frac{1}{(\exp(\frac{\hbar\omega}{k_B T}) - 1)}$. Thus the average internal

energy of the sample under thermal equilibrium is :

$$\begin{aligned}
E &= \sum_{\omega} (\langle n \rangle + \frac{1}{2}) \hbar \omega \\
&= 3N \int d\omega (\langle n \rangle + \frac{1}{2}) \hbar \omega \delta(\omega - \omega_E) \\
&= 3RT \left(\frac{1}{2} x_E + \frac{x_E}{e^{x_E} - 1} \right)
\end{aligned} \tag{2.5}$$

where $x_E = \frac{\hbar \omega_E}{k_B T}$. The Einstein model specific heat will hence be:

$$c_v = 3R \frac{x_E^2 \exp(x_E)}{(e^{x_E} - 1)^2} \tag{2.6}$$

We define $\theta_E = \frac{\hbar \omega_E}{k_B}$ as a scaling factor for the temperature known as the Einstein Temperature. In terms of θ_E the specific heat becomes:

$$c_v = 3R \left(\frac{\theta_E}{T} \right)^2 \frac{\exp(\theta_E/T)}{(e^{\theta_E/T} - 1)^2} \tag{2.7}$$

When the low-temperature limit is reached ($T \ll \theta_E$), c_v reduces to :

$$c_v = 3R \left(\frac{\theta_E}{T} \right)^2 \exp\left(\frac{\theta_E}{T}\right) + .. \tag{2.8}$$

and in the limiting case of very high temperatures ($T \gg \theta_E$):

$$c_v = 3R \left(1 - \frac{1}{12} \left(\frac{\theta_E}{T} \right)^2 + \dots \right) \tag{2.9}$$

which correctly reaches the classical value given by the Dulong and Petit law. When the low-temperatures limit was finally tested, it was found that the exponential decay does not agree with the experimental results. This was expected since in a strongly coupled system the atoms cannot all vibrate with the same fre-

quency. Recognizing this fact, many more realistic models have been developed first by Debye and later by Born-Von Karman and others.

2.2.3 The Debye Model

In this model the lattice vibrations are considered to be quantized and at low temperatures only vibrational modes of low frequencies are excited. These modes are characterized by phonons with long wavelengths in comparison to the thickness of the material. In this limit, the system must then behave like a continuum. Consequently, the use of continuum mechanics instead of atomistic description to determine the thermal properties of a low dimensional material at low temperatures is valid. Debye considered the system to be an elastic, isotropic continuum with a distribution function $D(\omega)$ of allowed frequencies. the average total vibrational thermal energy is:

$$E = 3 \int_0^{w_D} d\omega D(\omega) \left(\langle n \rangle + \frac{1}{2} \right) \hbar \omega \quad (2.10)$$

$$\text{with } D(\omega) = \frac{dn(k)}{d\omega} \quad (2.11)$$

To determine the energy of the system, we need to solve for $n(k)$, the number of allowed states and w_D the Debye cutoff frequency . Since the result is shape independent [117], we take a cube of side length L for convenience only. We begin with the the plane wave equation propagating in an isotropic medium.

$$\nabla^2 U = \frac{1}{v^2} \frac{\partial^2 U}{\partial t^2} \quad (2.12)$$

Where U is the displacement vector and v is the wave's velocity. The solutions that satisfy the boundary conditions are standing waves of the following form:

$$U(r, t) = \sin\left(\frac{n_x \pi x}{L}\right) \sin\left(\frac{n_y \pi y}{L}\right) \sin\left(\frac{n_z \pi z}{L}\right) \sin(\omega t) \quad (2.13)$$

Where n_x, n_y, n_z are positive integers related to the wave vectors of the wave vectors by $k_r = \frac{n_r \pi}{L}$ with $r = x, y, z$. The number of available states in the volume element $\Delta n = \Delta n_x \Delta n_y \Delta n_z$ of the n -space is:

$$\Delta n = \frac{L^3}{\pi^3} \Delta V_k = \frac{V}{\pi^3} \Delta V_k \quad (2.14)$$

Since n_r 's are confined to the first octant of n -space, $\Delta V_k = \Delta k_x \Delta k_y \Delta k_z$ is the volume of the first octant of the k -space. Taking this as the volume of the shell lying between k and $k+dk$ we obtain:

$$\Delta V_k = \frac{1}{8} (4\pi k^2) dk = \frac{1}{2} \pi k^2 dk \quad (2.15)$$

Substituting this into equation 2.14, gives the allowed number of states:

$$dn(k) = \frac{V}{\pi^3} \Delta V_k = \frac{V}{2\pi^2} k^2 dk \quad (2.16)$$

In the Debye model, the relation between the angular frequency ω and the wave vector k is linear:

$$\omega = vk \quad (2.17)$$

By replacing k by $\frac{\omega}{v}$ in the last equation, we arrive to the density of phonon modes for each polarization direction:

$$D(\omega) = \frac{dn(k)}{d\omega} = \frac{V}{2\pi^2} \frac{\omega^2}{v^3} \quad (2.18)$$

The cutoff frequency ω_D is obtained by assuming that the total number of modes in a solid should be equal to the number to atoms in it

$$3N = \frac{V}{2\pi^2} \frac{\omega_D^3}{v^3} \implies \omega_D = v \left(\frac{6\pi^2 N}{V} \right)^{(1/3)} \quad (2.19)$$

The characteristic Debye temperature is thus defined as :

$$\theta_D = \frac{\hbar\omega_D}{k_B} \quad (2.20)$$

This represents the separation between the low temperature regime where the atoms vibrate collectively as a solid from the classical regime in which atoms vibrate separately from each other. By introducing $D(\omega)$ and ω_D The average thermal energy becomes:

$$E = E_0 + \frac{3V(k_B T)^4}{2\pi^2 c^3 \hbar^3} \int_0^{x_D} \frac{x^3}{(e^x - 1)} dx \quad (2.21)$$

Where $E_0 = \frac{9N\hbar\omega_D}{8}$ is the zero point contribution and $x_D = \frac{\hbar\omega_D}{k_B T} = \frac{\theta_D}{T}$. Replacing with θ_D we obtain:

$$E = E_0 + 9Nk_B T \left(\frac{T}{\theta_D} \right)^3 \int_0^{x_D} \frac{x^3}{(e^x - 1)} dx \quad (2.22)$$

By taking the derivative of the energy with respect to the temperature we obtain the specific heat:

$$c_v = 9R \left(\frac{T}{\theta_D} \right)^3 \int_0^{x_D} \frac{x^4 e^x}{(e^x - 1)^2} dx \quad (2.23)$$

When the low-temperature limit is reached ($T \ll \theta_D$), c_v reduces to :

$$c_v = \frac{12\pi^4}{5} (R/\theta_D^3) T^3 = \beta T^3 \quad (2.24)$$

where $\beta = (1943.7/\theta_D^3) J/mol.K^4$. This is the universal Debye T^3 law which is well observed and tested for bulk materials at low-temperatures. In the limiting case of very high temperatures ($T \gg \theta_D$):

$$c_v = 3R \left(1 - \frac{1}{20} \left(\frac{\theta_D}{T} \right)^2 + \dots \right) \quad (2.25)$$

As the temperature increases c_v correctly reaches the Dulong and Petit limit of $3R$. Thus the Debye law gives a more accurate description of the thermal properties of materials at low temperatures than the Einstein's model.

2.3 Specific Heat Measurement Techniques at Low-temperatures

When an isothermal sample of specific heat $c(T)$ is subjected to a power $P(t)$ in adiabatic conditions during a time interval $t-t_0$, the sample heating would be described by:

$$\int_{t_0}^t P(t) dt = Q = \int_{T_0}^T c(T) dT \quad (2.26)$$

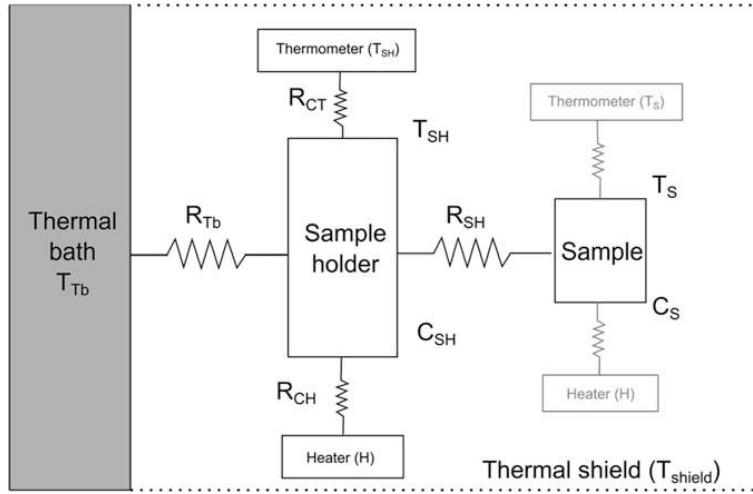


Figure 2.1: Scheme of the main elements of a calorimeter for measurements of heat capacity [2]

where Q is the total heat supplied to the sample during the time interval and T_0 the starting temperature of the system. We are interested in the evaluation of $c(T)$ when Q and T are determined. The apparatus which measures $c(T)$ at different temperatures is called a calorimeter. To determine the specific heat at low temperatures, first, the sample's temperature should be decreased to a starting low temperature of T_0 . Second, the sample should be isolated thermally from its environment. And finally an amount of heat Q should be supplied to it to reach a temperature T . In general, a low temperature calorimeter is designed according to figure 2.1 The calorimeter usually contains a platform on which the sample of specific heat c , a thermometer T_{sH} and a heater H are thermally connected by grease. The platform is linked to the thermal bath by a thermal resistance R_{Tb} , while the sample and the sample holder are joined by a thermal resistance R_{SH} . molecules (generally in the gas phase) adsorbed on a surface. Calorimeters can be categorized into isothermal, isoperibol, and adiabatic types depending on the heat transfer conditions between the sample holder and the thermal bath. In isothermal calorimeters, the calorimeter and the thermal bath are held at a

constant temperature T_{Tb} . If the bath only is isothermal then the mode of operation is called isoperibol as in AC calorimetry, relaxation calorimetry or dual slope calorimetry. Whereas in an adiabatic calorimeter as in heat pulse calorimetry, the exchange of heat between the calorimeter and the shield is kept negligible. However, these methods exhibit some deficiencies; the adiabatic method only applies to large samples (around 10g) and while the AC calorimetry solves this issue it still gives low accuracy measurements [118].

Another calorimetry used for small samples is the relaxation method developed by Bachmann et al. [119]. It consists of applying a heat pulse to the sample, and then analyzing the corresponding temperature response by solving the heat flow equations. The relaxation technique utilized by our work, is an extension to the method just mentioned, and takes into account the heat flow between the sample and the platform, which is defined as the Two-Tau effect.

2.4 Nanowires specific heat Model

The specific heat of nanowires differ from their bulk counterparts due to the contribution of the surface atoms in the heat transport process at low-dimensions [120]. Therefore, we will derive an expression for the specific heat of nanowires at low-temperatures following the Debye approximations. Within the theory of continuum mechanics the equation of an elastic wave can be expressed as:

$$\nabla^2 U = \frac{1}{v^2} \frac{\partial^2 U}{\partial t^2} \quad (2.27)$$

Where U is the displacement vector and v is the wave's velocity. In the case where the nanowires are fixed at $z=0$ and free at $z=L$, no axial stress is involved at $z=L$

i.e. $\sigma_z z = 0$ and $\frac{\partial U_z}{\partial z}|_{z=L} = 0$ and $U_z = 0$ at $z=0$. Also as boundary conditions, we consider azimuthal symmetry and we assume that the displacement is finite at $r=0$ and vanishes at $r=R$, R being the radius of the nanowire. Applying these boundary conditions and the separation of variables method we solve the equation of motion using cylindrical coordinates. we obtain the following displacement vector:

$$U(r, z, t) = \sum_{m=0}^{\infty} \sum_{n=1}^{\infty} J_m\left(\frac{z_{mn} \cdot r}{R}\right) \cdot \sin\left(\frac{(2n+1)\pi z}{2L}\right) e^{(-i\omega t)} \quad (2.28)$$

where z_{mn} are the zeros of the first kind Bessel's function J_m with $n = 1, 2, 3, \dots$ and n is a quantized integer. The total wavevector of the wave obtained from this derivation is:

$$k^2 = k_r^2 + k_z^2 = \left(\frac{z_{mn} \cdot r}{R}\right)^2 + \left(\frac{(2n+1)\pi}{2L}\right)^2 \quad (2.29)$$

2.4.1 Dispersion Relation

To obtain the dispersion relation of each mode we follow the analysis of Landau and Lifshitz in the theory of elasticity [121]. For nanowires three modes of vibration exist; longitudinal, torsional and bending each with a linear dispersion relation $w = vk$ as dictated by continuum mechanics.

Longitudinal mode: The equation of motion of a wire for simple extension or compression is the following :

$$\frac{\partial^2 U_z}{\partial z^2} - \frac{\rho}{E} \frac{\partial^2 U_z}{\partial t^2} = 0 \quad (2.30)$$

where ρ is the material's mass density and E is the Young's modulus for the nanowires. The wave's velocity is hence:

$$v_L = \sqrt{\frac{E}{\rho}} \quad (2.31)$$

Torsional mode: The equation of motion of a wire under torsional vibration is:

$$\frac{\partial^2 \phi}{\partial z^2} - \frac{\rho I}{C} \frac{\partial^2 \phi}{\partial t^2} = 0 \quad (2.32)$$

where ϕ is the angle of rotation of the cross section of the wire, I the moment of inertia of the area about its center of mass and C the torsional rigidity. The wave's velocity is

$$v_T = \sqrt{\frac{C}{\rho I}} \quad (2.33)$$

Bending mode: The equation of motion of a slightly bent wires in each of the x and y coordinate is the following:

$$\frac{\partial^2 X}{\partial t^2} - \frac{EI_y}{\rho S} \frac{\partial^4 X}{\partial z^4} = 0 \quad (2.34)$$

$$\frac{\partial^2 Y}{\partial t^2} - \frac{EI_x}{\rho S} \frac{\partial^4 Y}{\partial z^4} = 0 \quad (2.35)$$

where ρS is the mass per unit length of the wire with S being its cross-sectional area, and EI the flexural rigidity with $I_{x(y)}$ as the second moment of area. The velocity of the bending mode is :

$$v_{B1(2)} = 2k \sqrt{\frac{EI_{x(y)}}{\rho S}} \quad (2.36)$$

By replacing each velocity and the total wavevector we obtain the following dispersion relations:

$$\omega_L^2 = \frac{E}{\rho} \pi^2 \left(\left(\frac{z_m}{\pi R} \right)^2 + \left(\frac{2n+1}{2L} \right)^2 \right) \quad (2.37)$$

$$\omega_T^2 = \frac{C}{\rho I} \pi^2 \left(\left(\frac{z_m}{\pi R} \right)^2 + \left(\frac{2n+1}{2L} \right)^2 \right) \quad (2.38)$$

$$\omega_{B1}^2 = \frac{4EI_x}{\rho S} \pi^2 \left(\left(\frac{z_m}{\pi R} \right)^2 + \left(\frac{2n+1}{2L} \right)^2 \right)^2 \quad (2.39)$$

$$\omega_{B2}^2 = \frac{4EI_y}{\rho S} \pi^2 \left(\left(\frac{z_m}{\pi R} \right)^2 + \left(\frac{2n+1}{2L} \right)^2 \right)^2 \quad (2.40)$$

2.4.2 Density of states

Let's consider now Eq.2.37 which describes the dispersion relation of the longitudinal modes. According to Eq.2.37, the number of longitudinal modes with frequencies less than ω is equal to the number of lattice points (z_{mn} and $2n+1$) which obey:

$$\frac{E}{\rho} \pi^2 \left(\left(\frac{z_m}{\pi R} \right)^2 + \left(\frac{2n+1}{2L} \right)^2 \right) \leq \omega^2 \quad (2.41)$$

that is, the number of points lying within an octant of the ellipse given by :

$$\frac{x^2}{\pi^2 R^2} + \frac{y^2}{4L^2} = \frac{\rho \omega^2}{E \pi^2} \quad (2.42)$$

The nanowires investigated in this work are large enough to consider this number equal to the actual area of the first octant of the ellipse. Therefore, the number

of longitudinal modes of frequencies less than ω in the nanowires is given by:

$$N_L(\omega) = \frac{RL\rho\omega^2}{2E} \quad (2.43)$$

Following the same derivation, the number of torsional modes with frequencies less than ω in the nanowires is found to be:

$$N_T(\omega) = \frac{RL\rho I\omega^2}{2c} \quad (2.44)$$

and the number of bending modes with frequencies less than ω is equal to twice (because of the isotropic nature of the x=y plane and the degeneracy of the bending modes) the volume of the first octant of the ellipsoid specified by:

$$\frac{x^2}{\left(\frac{\omega^2 R^4 \rho S}{4EI}\right)} + \frac{y^2}{\left(\frac{4\omega^2 L^4 \rho S}{\pi^4 EI}\right)} + \frac{z^2}{\left(\frac{\omega^2 L^2 R^2 \rho S}{2\pi^2 EI}\right)} = 1 \quad (2.45)$$

that is:

$$N_B(\omega) = \frac{(\omega RL\sqrt{\rho S})^3}{3\sqrt{2}\pi^2(EI)^{\frac{3}{2}}} \quad (2.46)$$

The total number of modes in the nanowires is thus:

$$N_{Total} = 3pN_c = \frac{RL\rho}{2} \left(\frac{I}{C} + \frac{1}{E} \right) \omega_{D1}^2 + \frac{(RL\sqrt{\rho S})^3}{3\sqrt{2}\pi^2(EI)^{\frac{3}{2}}} \omega_{D2}^3 \quad (2.47)$$

where p is the number of atoms per unit cell, N_c is the total number of unit cells, and $\omega_{D1(2)}$ are the cut-offs frequencies for linear (quadratic) dispersions. It is common practice to relate the cut-off frequency to the Debye temperature according to $\theta_D = \frac{\hbar\omega_D}{k_B}$ where k_B is the Boltzmann constant. This allows us to establish two Debye temperatures for the nanowires: a Debye temperature for

the modes of linear dispersions given by:

$$\theta_{D,L}^2 = \frac{3pN_c\hbar^2}{RL\rho\left(\frac{I}{C} + \frac{1}{E}\right)k_B^2} \quad (2.48)$$

and a Debye temperature for the modes of quadratic dispersions given by:

$$\theta_{D,Q}^3 = \frac{9pN_c\hbar^3\pi^2(EI)^{\frac{3}{2}}}{\sqrt{2}(RL(\rho S)^{\frac{1}{2}}k_B)^3} \quad (2.49)$$

The phonon density of states $g(\omega)$ is given by:

$$g(\omega)d\omega = (N(\omega + d\omega) - N(\omega)) = N'(\omega)d\omega \quad (2.50)$$

In the limit where $d\omega$ tends to zero,

$$g(\omega) = RL\rho\left(\frac{I}{C} + \frac{1}{E}\right)\omega_{D1} + \frac{(RL\sqrt{\rho S})^3}{\sqrt{2}\pi^2(EI)^{\frac{3}{2}}}\omega_{D2}^2 \quad (2.51)$$

It can be clearly noticed from Eq.2.51 that the density of states in the nanowires is the sum of densities of surface-like states(first term in Eq.2.51) and volume-like states (second term in Eq.2.51).

2.4.3 Specific Heat

At this point, it is possible to calculate the nanowire's specific heat in terms of its length and radius from:

$$c = \int_0^{\omega_{D1}} \frac{\hbar^2 \omega^2}{k_B T^2} \frac{e^{\frac{\hbar \omega}{k_B T}}}{(e^{\frac{\hbar \omega}{k_B T}} - 1)^2} g_1(\omega) d\omega + \int_0^{\omega_{D2}} \frac{\hbar^2 \omega^2}{k_B T^2} \frac{e^{\frac{\hbar \omega}{k_B T}}}{(e^{\frac{\hbar \omega}{k_B T}} - 1)^2} g_2(\omega) d\omega \quad (2.52)$$

where $g_1(\omega)$ and $g_2(\omega)$ are the first and second terms in Eq.2.51. Upon introducing the dimensionless variable $x = \frac{\hbar \omega}{k_B T}$ and the expressions of the Debye temperature (Eq.2.48 and Eq.2.49), we can write the expression of the nanowires specific heat as follows:

$$c = 3pN_c k_B \left(\frac{T}{\theta_{D,L}} \right)^2 \int_0^{\frac{\theta_{D,L}}{T}} \frac{x^3 e^x}{(e^x - 1)^2} dx + \frac{9}{2} pN_c k_B \left(\frac{T}{\theta_{D,Q}} \right)^3 \int_0^{\frac{\theta_{D,Q}}{T}} \frac{x^4 e^x}{(e^x - 1)^2} dx \quad (2.53)$$

The first and second term in Eq.2.53 describe contributions to the specific heat from modes of linear and quadratic dispersions respectively. In the limit of low temperatures, the upper bound of the integral tends to infinity and the expression of the nanowire's specific heat reduces to:

$$c = 3pN_c k_B \times 7.212 \times \left(\frac{T}{\theta_{D,L}} \right)^2 + \frac{9}{2} pN_c k_B \times 25.980 \times \left(\frac{T}{\theta_{D,Q}} \right)^3 \quad (2.54)$$

which explains the deviation of the nanowire's specific heat from the Debye T^3 law.

2.5 Clamped Graphene specific heat Model

Many theoretical models have been developed for the determination of the thermal properties of graphene [5, 75, 83, 87, 122]. In our work we will adopt the semi-continuum model from [84] for graphite and modify it to account for the clamped effect of the graphene sample. We assume that graphite is formed of N two-dimensional elastic sheets with negligible inter-layer friction. Within the theory of continuum mechanics, the equation of vibration of a graphite sample is expressed as:

$$D\nabla^2\omega + \rho h \frac{\partial^2\omega_i}{\partial t^2} = q_i \quad i = 1, 2 \dots N \quad (2.55)$$

Where D is the bending stiffness of each sheet, ω_i is the deflection of the i th sheet, ρ the mass density of the sheet, h its thickness and q_i the pressure applied to an atomic sheet due to the interlayer Van der Waals interaction (vdW). For infinitesimal vibration, the net pressure due to the vdW interaction is assumed to be proportional to the deflection between two layers, in other words:

$$q_i = \sum_{j=1}^N c_{ij}(\omega_i - \omega_j) = \omega_i \sum_{j=1}^N c_{ij} - \sum_{j=1}^N \omega_j c_{ij} \quad (2.56)$$

where c_{ij} are the vdW interaction coefficients and N the total number of layers in graphite. Supposing a is the length of a graphene sheet and b its width, the deflection of all the layers can be approximated by a periodic solution as follows:

$$\omega_k(x, y, t) = A_k \sin\left(\frac{m\pi x}{a}\right) \sin\left(\frac{n\pi y}{b}\right) e^{i\omega t} \quad (2.57)$$

with A_k being N unknowns coefficients, m and n positive integers and ω the angular frequency. Replacing Eq. 2.56 and Eq. 2.57 into Eq.2.55, we obtain

$$\left\{ D \left[\left(\frac{m\pi}{a} \right)^2 + \left(\frac{n\pi}{b} \right)^2 \right]^2 - \sum_{j=1}^N c_{kj} - \rho h \omega^2 \right\} A_k + \sum_{j=1}^N c_{kj} A_j = 0 \quad (k = 1, 2, \dots, N) \quad (2.58)$$

2.5.1 Dispersion Relation

The lattice vibrations of graphite can be separated into three polarizations; in-plane transverse, in-plane longitudinal, and out-of-plane mode. The dispersion relations corresponding to these modes are obtained by Nihira and Iwata [83] by employing the semi-continuum model described above from :

$$\omega_l^2 = v_l^2 (k_x^2 + k_y^2) + \left(\frac{4\zeta}{c^2} \sin^2 \left(\frac{ck_z}{2} \right) \right) \quad (2.59)$$

$$\omega_t^2 = v_t^2 (k_x^2 + k_y^2) + \left(\frac{4\zeta}{c^2} \sin^2 \left(\frac{ck_z}{2} \right) \right) \quad (2.60)$$

$$\omega_z^2 = \kappa^2 (k_x^2 + k_y^2)^2 + 4\mu^2 \sin^2 \left(\frac{ck_z}{2} \right) + \zeta (k_x^2 + k_y^2) \quad (2.61)$$

where ω is the angular frequency, k_x and k_y are the wave vectors, and the subscripts l , t , and z refer to the in-plane longitudinal and transverse mode, and the out-of-plane mode, respectively. v_l and v_t are the wave velocities, c the inter-layer spacing, and ζ and μ are two constants related to elastic constants c_{ij} . For a single layer of graphene, $k_z = 0$ and the dispersion relations become:

$$\omega_l = v_l \sqrt{(k_x^2 + k_y^2)} = v_l k \quad (2.62)$$

$$\omega_t = v_t \sqrt{(k_x^2 + k_y^2)} = v_t k \quad (2.63)$$

$$\omega_z = \sqrt{\kappa^2 (k_x^2 + k_y^2)^2 + \zeta (k_x^2 + k_y^2)} \quad (2.64)$$

The in-plane transverse and longitudinal phonon polarizations admit a linear expressions ($\omega = v_g K$, v_g being the group velocity of the wave) whereas the out-of-plane dispersion relation is approximately quadratic ($\omega = \alpha k^2$). But, since our graphene sample is clamped to its holder, the out-of-plane mode is assumed to be suppressed and we no longer take into account its contribution to the density of states and hence the specific heat. The wavevector k of this two-dimensional material deduced from 2.57 would be:

$$k^2 = k_x^2 + k_y^2 = \left(\frac{m\pi x}{a}\right)^2 + \left(\frac{n\pi y}{b}\right)^2 \quad (2.65)$$

2.5.2 Density of states

Let's consider now Eq.2.62 which describes the dispersion relation of the longitudinal modes. According to Eq.2.62, the number of longitudinal modes with frequencies less than ω is equal to the number of lattice points (n and m) which obey:

$$\pi^2 v_l^2 \left(\left(\frac{m}{a}\right)^2 + \left(\frac{n}{b}\right)^2 \right) \leq \omega^2 \quad (2.66)$$

that is, the number of points lying within an octant of the ellipse given by :

$$\frac{m^2}{a^2} + \frac{n^2}{b^2} = \frac{\omega^2}{v_l^2 \pi^2} \quad (2.67)$$

The graphene samples investigated in this work are large enough to consider this number equal to the actual area of the first octant of the ellipse. Therefore, the number of longitudinal modes of frequencies less than ω in graphene is given by:

$$N_L(\omega) = \frac{A}{4\pi} \left(\frac{\omega}{v_l}\right)^2 \quad (2.68)$$

With A being the area of the graphene sample. Following the same derivation, the number of transverse modes with frequencies less than ω in graphene is found to be:

$$N_t(\omega) = \frac{A}{4\pi} \left(\frac{\omega}{v_t} \right)^2 \quad (2.69)$$

It is common practice to relate the cut-off frequency to the Debye temperature according to $\theta_D = \frac{\hbar\omega_D}{k_B}$ where k_B is the Boltzmann constant. This allows us to establish a Debye temperature for the clamped graphene: a Debye temperature for the modes of linear dispersions is given by:

$$\theta_{D,L}^2 = \frac{24N\pi\hbar^2v^2}{Ak_B^2} \quad (2.70)$$

v^2 being the effective sum of the longitudinal and transverse velocities. The phonon density of states $g(\omega)$ is given by:

$$g(\omega)d\omega = (N(\omega + d\omega) - N(\omega)) = N'(\omega)d\omega \quad (2.71)$$

In the limit where $d\omega$ tends to zero,

$$g(\omega)_L = \frac{A\omega}{2\pi v^2} \quad (2.72)$$

It can be clearly noticed that the density of states of the in-plane modes is linear in the frequency.

2.5.3 Specific Heat

At this point, it is possible to calculate the clamped graphene's specific heat:

$$c = \int_0^{\omega_{D1}} \frac{\hbar^2 \omega^2}{k_B T^2} \frac{e^{\frac{\hbar \omega}{k_B T}}}{(e^{\frac{\hbar \omega}{k_B T}} - 1)^2} g_L(\omega) d\omega \quad (2.73)$$

Upon introducing the dimensionless variable $x = \frac{\hbar \omega}{k_B T}$ and the expression of the Debye temperature, we can write the expression of the clamped graphene's specific heat as follows:

$$c = 12Nk_B \left(\frac{T}{\theta_{D,L}} \right)^2 \int_0^{\frac{\theta_{D,L}}{T}} \frac{x^3 e^x}{(e^x - 1)^2} dx \quad (2.74)$$

This describes the contribution to the specific heat from modes of linear dispersions only. In the limit of low temperatures, the upper bound of the integral tends to infinity and the expression of the clamped graphene's specific heat reduces to:

$$c = 12Nk_B \times 7.212 \times \left(\frac{T}{\theta_{D,L}} \right)^2 \quad (2.75)$$

Therefore, a clamped graphene sample's low-temperature specific heat is essentially that of a two-dimensional material.

Chapter 3

Experimental Study

The thermal properties of the materials have been evaluated by means of heat calorimetry. The apparatus used was The Physical Property Measurement System (PPMS) Dynacool developed by Quantum Design. The instrument offers a large variety of options for the calculation of different physical properties such as thermal conductivity, seebeck coefficient and specific heat among others. In our work, the study is solely focused on the determination of the heat capacity and thermal conductance of the samples. The measurement of heat capacity provides important knowledge about the electronic, magnetic and lattice properties of the materials. It is especially useful when it comes to the implementation of the characterized materials in thermal devices.

The PPMS system is equipped with diverse measurement techniques that are optimized for different sample sizes and high accuracy requirements. The robust analytical skills of the system uses relaxation time techniques to determine the specific heat and thermal conductance of the sample. A simple one-tau model [123] is employed when there's strong thermal coupling between the sample and the sample platform, whereas a two-tau model developed by Hwang, Lin,

and Tien [124] is used when we have poor thermal transport and the effect of the interface should be taken into account. In our work, we develop a "Three-tau model" to determine of the specific heat of the free surface ZnO nanowires and the thermal conductance of the interface separating the ZnO nanowires and the Silicon substrate.

3.1 Analysis Methods

In the following, the different computational models employed by the PPMS for the determination of the specific heat and thermal conductance of bulk materials are elaborated. We also present the new model for the calculation of the thermal properties of nanowires.

3.1.1 One-Tau Model

This mode is utilized when no sample is mounted on the platform or when perfect thermal coupling exists between the sample and the platform. These cases are illustrated in Figure 3.1 Due to conservation of energy the difference in the power entering and exiting the sample should be equal to the thermal response of the sample.

$$P_{in}(t) - P_{out}(t) = \frac{dQ}{dt} \quad (3.1)$$

Knowing that the heat capacity is defined as:

$$c_p = \left. \frac{dQ}{dT} \right|_p \quad (3.2)$$

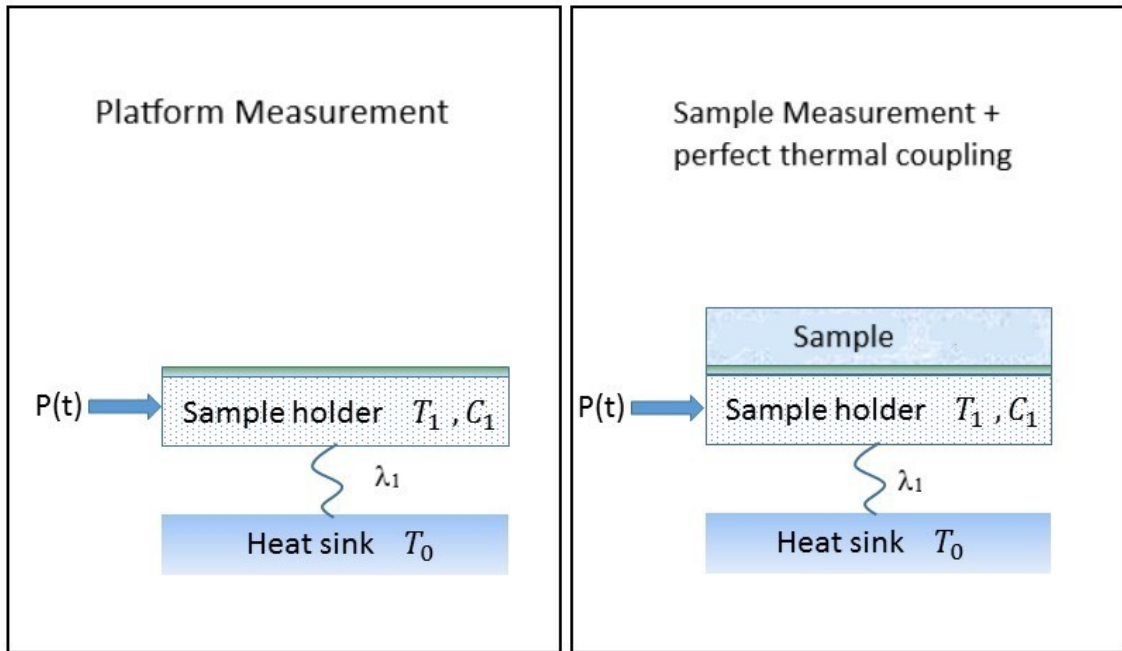


Figure 3.1: Heat flow diagram for the one tau simple model cases.

And that by Fourier's Law of heat conduction:

$$P_{out}(t) = \lambda_1(T_1 - T_0) \quad (3.3)$$

We obtain the heat balance equation:

$$P(t) = c_1 \frac{dT_1}{dt} + \lambda_1(T_1 - T_0) \quad (3.4)$$

where: c_1 is the total heat capacity of the sample and sample platform, λ_1 the thermal conductance of the wires ($W.K^{-1}$), T_0 the temperature of the thermal bath (puck frame), T_1 the temperature of the platform at time t , and $P(t)$ the input power in the sample platform.

During the experiment, constant power is applied in a pulse which causes a rise

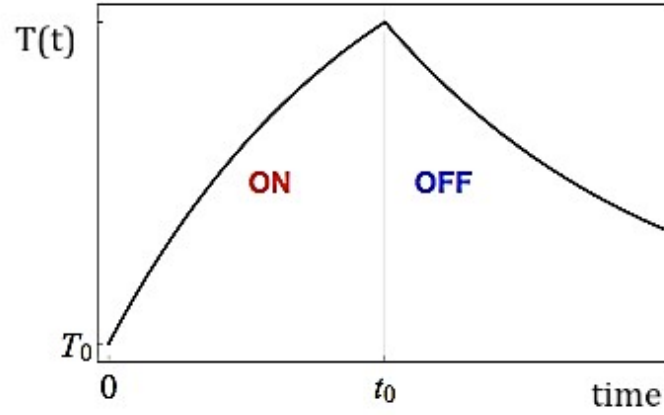


Figure 3.2: Heat pulse calorimetry principle. Heat is applied till $t = t_0$, after which the temperature starts to relax exponentially

in the temperature of the sample in measurement. Then the power is turned off, and at this point the temperature starts to decrease exponentially (figure 3.2).

The solution to the differential equation with heater on and heater off portions is:

$$\begin{aligned}
 T_{on}(t) &= \frac{P_0}{c}\tau(1 - e^{-\frac{t}{\tau}}) + T_0 \quad \text{for } (0 \leq t \leq t_0) \\
 T_{off}(t) &= \frac{P_0}{c}\tau(1 - e^{-\frac{t_0}{\tau}})e^{-\frac{-(t-t_0)}{\tau}} + T_0 \quad \text{for } (t > t_0)
 \end{aligned}
 \tag{3.5}$$

where $\tau = \frac{c_1}{\lambda_1}$. The unknowns c_1 , λ_1 and T_0 are determined by nonlinear least square fitting of the temperature curve with the data [125].

3.1.2 Two-Tau Model

This more sophisticated model is applied when the thermal contact between the sample and the platform is weak. In other words, the Heat Capacity software of the system takes into account a temperature difference between the sample and its holder and introduces the thermal conductance λ_2 between them as shown in figure 3.3 .

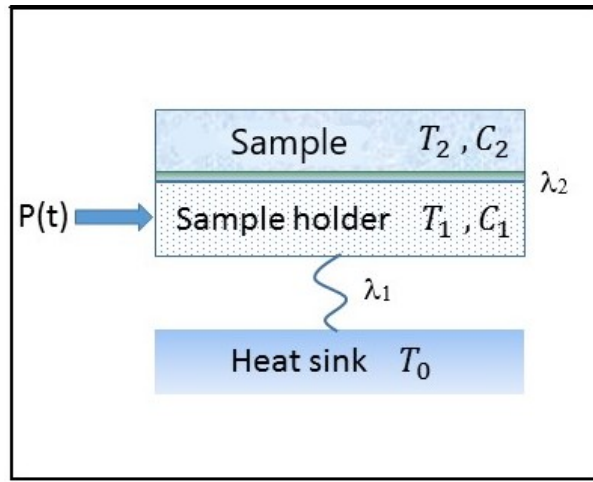


Figure 3.3: Heat flow diagram for the two-tau model.

The heat balance equations become:

$$\begin{cases} P(t) = c_1 \frac{dT_1(t)}{dt} + \lambda_1(T_1(t) - T_0) + \lambda_2(T_1(t) - T_2(t)) & (3.6) \\ 0 = c_2 \frac{dT_2(t)}{dt} + \lambda_2(T_2(t) - T_1(t)) & (3.7) \end{cases}$$

where c_1 is the specific heat of the addenda (platform + applied grease), c_2 the specific heat of the sample, λ_2 the thermal conductance of the Apiezon N grease, and $T_2(t)$ is the temperature of the sample at instant t . In the case of graphene sample, c_2 would be its specific heat and λ_2 the thermal conductance of the interface between graphene and the platform (no grease).

Equation 3.6 depicts the flow of heat from the heat sink to the platform and from the platform to the sample. Whereas equation 3.7 represents the heat flow to the sample.

It is difficult to directly solve these equations as in the one-tau model so instead we refer to fitting methods. Hwang, Lin, and Tien [124] have showed that we can transform the two differential equations into a set of three equations with c_2 , λ_2 , λ_1 unknowns and c_1 determined from the simple model measurement. By fitting the raw data to the temperature difference $\Gamma(t) = T_1(t) - T_0$ one can solve the three coupled equations to obtain the value of the heat capacity of the sample.

3.1.3 Three-Tau Model

In order to determine the heat capacity of the nanowires, we assume a temperature difference between the wires and the substrate in addition to the two-tau interaction between the substrate and the platform as shown in figure 3.4. The heat balance equations become the following:

$$\left\{ \begin{array}{l} P(t) = c_1 \frac{dT_1(t)}{dt} + \lambda_1(T_1(t) - T_0) + \lambda_2(T_1(t) - T_2(t)) \quad (3.8) \\ 0 = c_2 \frac{dT_2(t)}{dt} + \lambda_2(T_2(t) - T_1(t)) + \lambda_3(T_2(t) - T_3(t)) \quad (3.9) \\ 0 = c_3 \frac{dT_3(t)}{dt} + \lambda_3(T_3(t) - T_2(t)) \quad (3.10) \end{array} \right.$$

where where c_3 is the specific heat of the nanowires, c_2 the specific heat of the substrate, λ_3 the thermal conductance of the interface between the silicon substrate and ZnO nanowires, and $T_3(t)$ is the temperature of the ZnO nanowires at instant t . Equation 3.10 represents the flow of heat to and from the nanowires when the power is on and off. Following the two-tau model we transform the three equations into one of third differential and integrate over the measurement

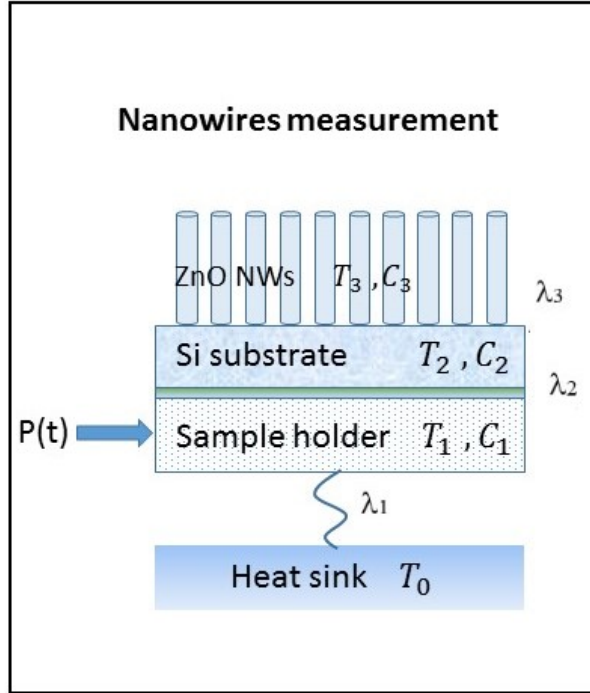


Figure 3.4: Heat flow diagram for the three-tau model

period. Then by fitting the resulting equation for $T_1(t)$ to the thermal response of the calorimeter using least squares method, we obtain the values of c_3 and λ_3 . A detailed derivation of the model is found in appendix A.

3.2 Experimental Setup

The experiment was conducted on samples of Zinc Oxide nanowires on Silicon substrates that were synthesized in the Laboratory of Nanotechnology, Instrumentation and Optics (LNIO), at the University of Technology of Troyes (UTT), and on commercial graphene samples. The PPMS calorimetric measurements were performed at the Central Research Science Laboratory (CRSL), at the American University of Beirut (AUB).

3.2.1 Nanowires Sample Synthesis

The synthesis of well-aligned Zinc Oxide nanowires with controlled diameter size is conducted in two steps; the formation of a seed layer of ZnO and then the growth of the nanowires on it.

The ZnO seed layer of 15-20 nm thick is formed by ZnO nanoparticles that act as a nucleation agent for the growth of the ZnO nanowires on the layer. It is obtained by first dissolving 2.197 g of zinc acetate ($Zn(CH_3COO)_2 \cdot 2H_2O$) in 20 ml of ethanol with constant stirring for 24 hours. Second the solution obtained is spin-coated onto a clean Silicon substrate. Finally, the formed layer is annealed at $400^\circ C$ on a hot plate for a duration of 10 minutes. The spin-coating process is again repeated twice followed by annealing of the sample after each step.

The growth of ZnO nanowires on the seed layer is conducted by chemical bath deposition technique. 0.025 M of Zinc Acetate is dissolved in 250 ml of deionized water with stirring for a few minutes. Then 0.3 ml of ammonium hydroxide with a concentration of 28% is added to the solution under constant stirring. This solution is then heated up to $87^\circ C$ in a three-neck flask as shown in figure 3.5. After attaining this temperature, for a period of 15 minutes the Si substrate with the ZnO seed layer is introduced into the solution in order to grow the nanowires. In the end, the sample is thoroughly cleansed with deionized water.

The morphology and size of the nanowires can be controlled by varying the concentration of zinc acetate in the solution [126], or the dipping time in the synthesis process. In our work three samples referred as WP1 (d=101 nm), WP2 (d=85 nm) and WP3 (d=50 nm) were selected for the calorimetric measurements.

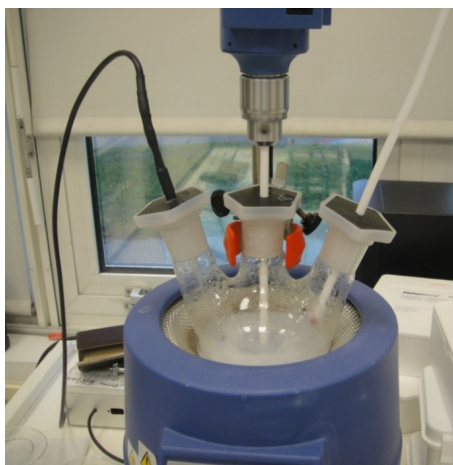


Figure 3.5: ZnO nanowires synthesis setup

3.2.2 Nanowires Sample Characterization

Scanning electron microscopy was conducted to demonstrate the different diameters of the selected samples. Top view electron micrographs are shown in figure 3.6

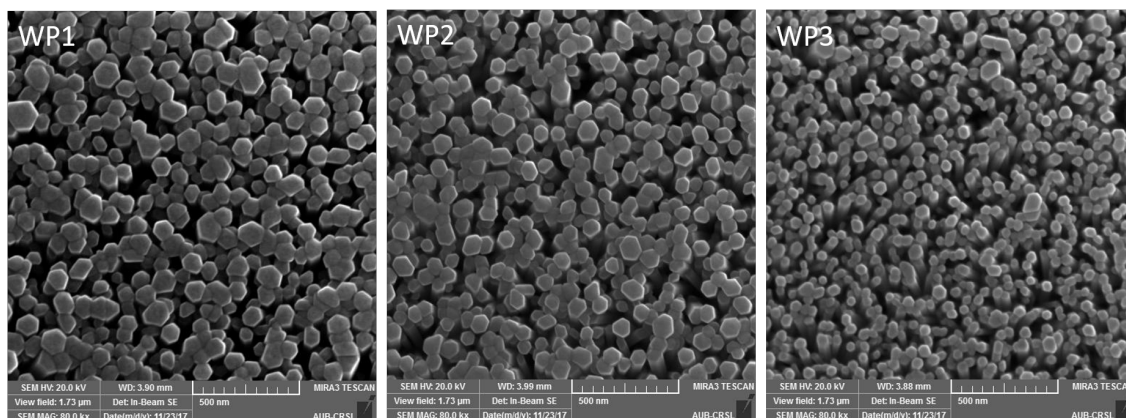


Figure 3.6: Scanning electron microscopy image of the samples investigated

X-ray diffraction was also performed on the synthesized samples to confirm their composition and determine their crystallinity. Figure 3.7 shows X-ray diffraction patterns for the different samples. The pattern indicates mono-crystallinity of

the ZnO nanostructures with the absence of other compounds. It also shows that the nanowires are grown with a preferential orientation along the [002] crystallographic direction. The peaks obtained in the X-ray diffraction patterns can be indexed to the hexagonal ZnO wurtzite structure.

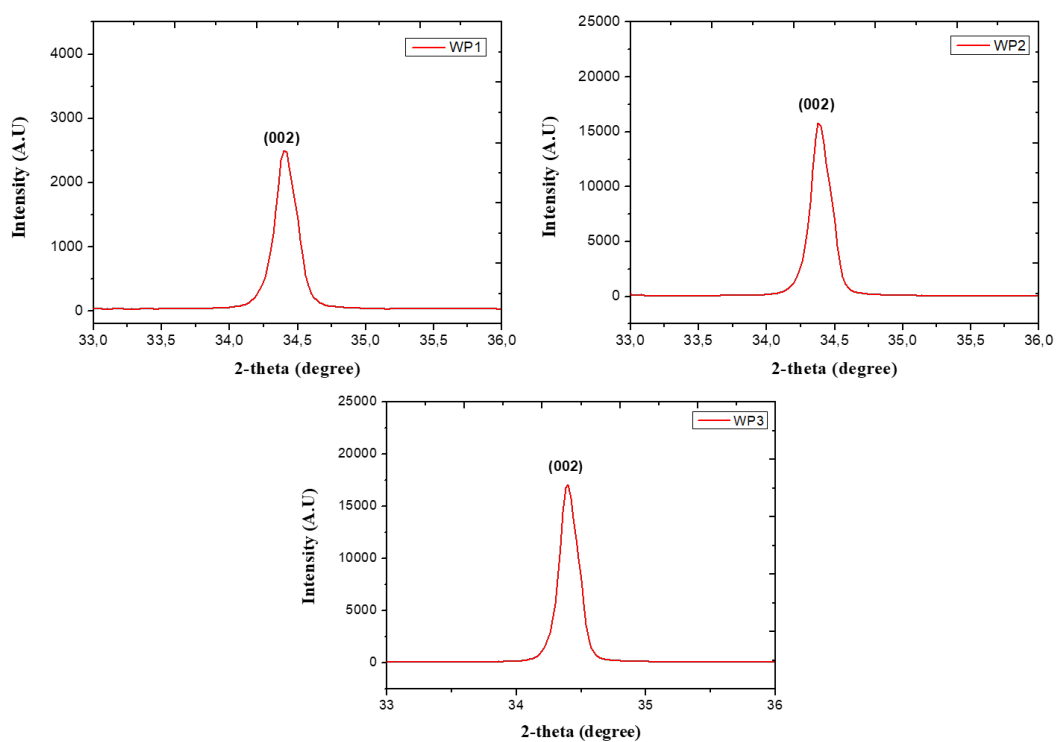


Figure 3.7: X-ray diffraction pattern of the samples investigated

3.2.3 Calorimetric Measurement

Setup Description

The Dynacool Physical Properties Measuring System is described schematically in figure 3.8. One of its main features is the double stage pulse tube coolers

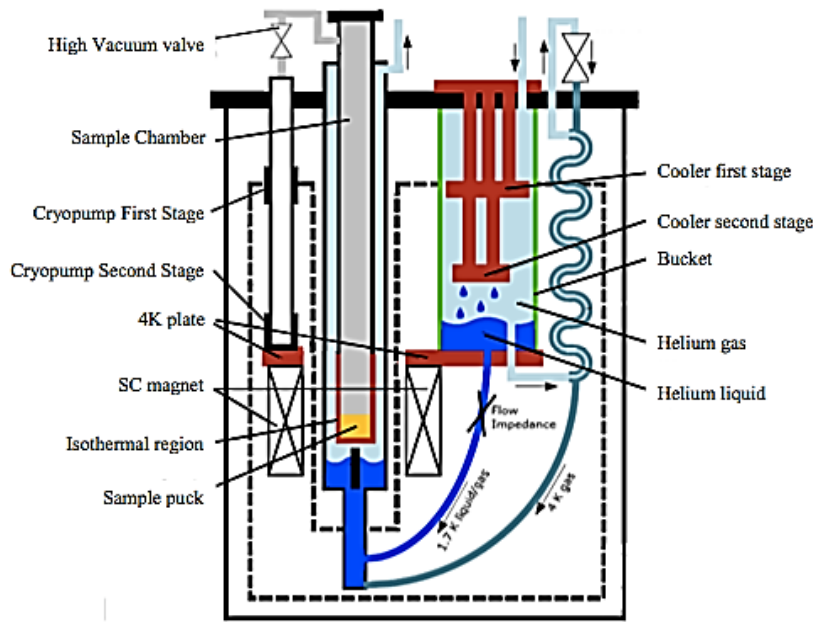


Figure 3.8: Dynacool simplified schematic drawing. [3]

that operate without the need of transfer of liquid cryogens. Instead, they make use of a small amount of liquid helium at the bottom of the bucket to cool the superconducting magnet to 4k.

The temperature of the system can be varied from 1.8k to 400k. This is controlled by first inserting liquid Nitrogen to cool down the system to a point where liquid helium won't evaporate, then combining liquid and gaseous helium and transporting them from the bucket to a cooling annulus surrounding the sample chamber. To ensure maximum efficiency in thermal properties measurement mode, the sample is placed in a thermally isolated chamber under high vacuum conditions

(< 10^{-6}Torr). Hence, the heat exchange between the sample and the environment is limited and the sample is protected from exterior heating from warmer surfaces. The vacuum pump of the PPMS is a cryogenic pump that operates in two stages; the first operates at 70k and the second at 4k. When the system reaches 4k the cryogenic pump equipped with charcoal absorbs any remaining gas in the sample chamber. Once specific heat measurement mode is established, the sample chamber pressure drops automatically to 5 Torr and then high vacuum is reached within a few seconds by sealing the chamber and opening the valves to expose it to the cryostat.

The PPMS also employs a puck which is a sample platform that provides thermal and electrical contact once placed in the sample chamber. Embedded in the puckframe is a thin sapphire (Al_2O_3) platform of $3 \times 3 \text{ mm}^2$ on which the sample is placed. A heater and a thermometer are mounted on the backside of the platform. The platform is connected to the puckframe with eight Au-Pd wires. Four wires are for the heater and four wires for the thermometer. The puck is shown in figure 3.9.

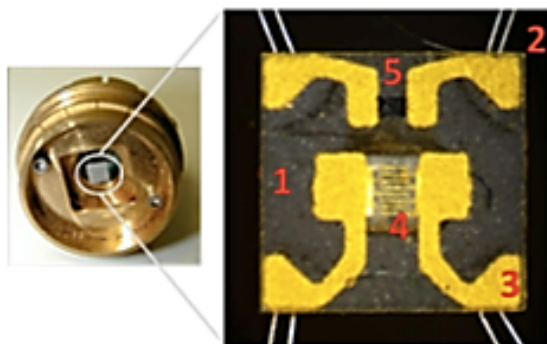


Figure 3.9: The puck 1792 (left) and the platform (right). 1: The sapphire platform 2: Au-Pd wires 3: Gold contacts 4: Thermometer 5: Heater. [4]

Table 3.1: The structural characteristics of the ZnO nanowires in the measured samples.

Sample	Average diameter (nm)	Average length (μm)
WP1	101	1.265
WP2	85	1.397
WP3	50	0.621

Measurement Procedure

Using a Talentool diamond cutter, these samples have been cut into small cubes that have a size of $3 \times 3 \text{ mm}^2$ approximately, with the nanowires masses ranging from 5 to 25 mg and the graphene's mass equals to 6.8ng on average. The structural characteristics of the zinc oxide nanowires are listed in table 3.1. To ensure stabilization of the sample on the platform, the puck is placed in a sample mounting station connected to a small vacuum pump and fixed in position with an interlock arm. Few milligrams of Apiezon N Grease is applied on the platform and the sample is placed on top of it.

For the nanowires, a first specific heat measurement is performed for the addenda (platform +grease) in order to separate the contribution of the sample from the total specific heat of the system. Then we measure the thermal properties of the Si substrate by itself after which we run the zinc oxide nanowires samples. As for the graphene, the calibration measurement is made for the platform by itself (no grease) and then the specific heat of the graphene sample is determined.

A measurement cycle begins by applying a heat pulse to the sample till a set temperature is reached at time t_0 . Then the heater is turned off and the sample is left to cool down. The temperature response curve is shown in Figure 3.2. The

temperature response curves are then fitted to the thermal calculation models developed in section 3.1. The addenda curves are fitted to the one-tau model and the specific heat of the addenda c_1 and the thermal conductance of the wires λ_1 are thus determined. While the curves for the graphene and Si substrate are fitted to the two-tau model to determine the specific heat c_2 and in the case of Si Substrate, the thermal conductance λ_2 between the substrate and the grease. The three-tau model is employed to fit the temperature curves of the zinc oxide nanowires, from which their specific heat c_3 and the thermal conductance λ_3 between the wires and the substrate are found.

Chapter 4

Results and Discussion

4.1 Specific heat Measurement

The specific heat measured in the experiment is that at constant pressure because measurements of constant volume specific heat are difficult to reproduce experimentally. But since the specific heat at constant volume is easier to describe in quantifiable models we employ it in our analysis instead of heat capacity at constant pressure. The interchange between the two is justifiable at room temperature and below since the difference between them is smaller as explained in section 2.1.

4.1.1 Addenda Measurement

As mentioned before, measuring the specific heat of the platform and the grease is important to determine the contribution of the sample separated from the addenda. Therefore a measurement of the empty puck and that of the puck with a known mass of grease are performed. We obtain the specific heat of the grease by subtracting the results of the addenda from those of the empty puck.

Four different combinations of measurements were made to obtain an average result for the specific heat of Apiezon N Grease(Addenda#1-empty Puck#1, Addenda#2-empty Puck#1, etc...) as shown in Figure 4.1. The solid line in Figure 4.2 represents the average specific heat and the shaded area around it is the uncertainty in the mean. [4]

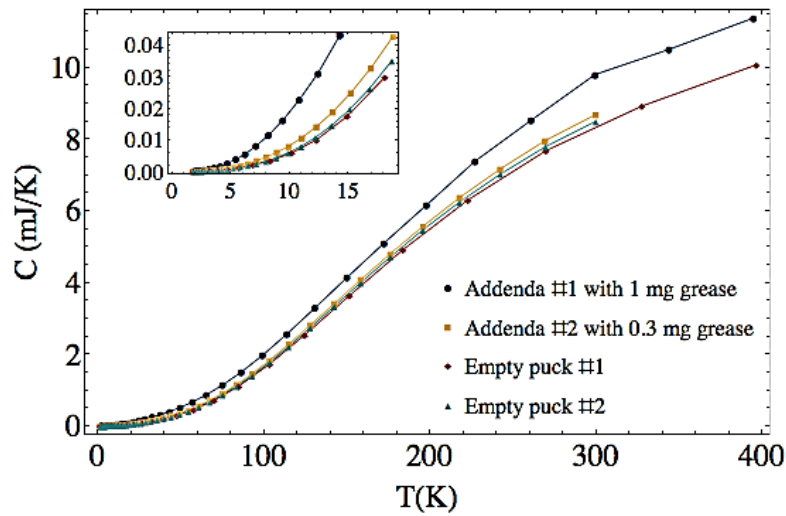


Figure 4.1: Heat capacity of the addenda and the empty puck; puck + 1mg of grease is shown in 'blue circles', puck+ 0.3mg of grease is shown in 'yellow square', empty puck is shown twice in 'red diamonds and green triangles'. [4]

4.1.2 Substrate Measurement

The Silicon substrate's specific heat has been measured for the purpose of comparison with the total specific heat of the substrate in the presence of nanowires. This is to prove that the existence of the Zinc Oxide nanowires on the Silicon substrate alters the thermal response of the calorimeter. The temperature curves

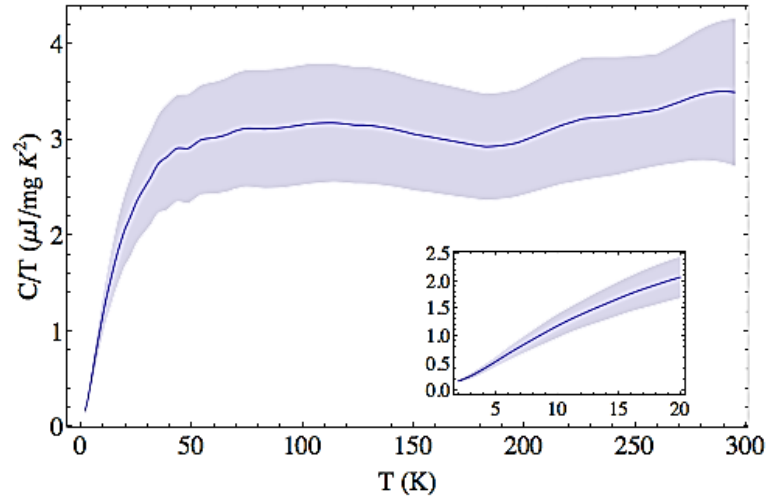


Figure 4.2: Average specific heat of the Apiezon N grease (solid blue line) with its uncertainty (shaded area). The inset shows the low temperature behavior. [4]

of the samples under investigation were fitted using the two-tau model developed in section 3.1. The measurement uncertainties are estimated to be of a value of 2% maximum due to the scatter in the data points.

Figure 4.3 shows a significant difference between the specific heat of the Si Substrate alone and that of the samples WP1, WP2 and WP3. Thus we conclude that the thermal properties of the nanowires are measurable with the means of this calorimetric technique.

4.1.3 ZnO nanowires measurements

The results of the specific heat of the zinc oxide nanowires for the three different synthesized samples WP1, WP2 and WP3 are shown in figure 4.4. The uncertainties in the measurements' data are estimated to be 10%; they arise from the scatter in the data points in each calculation and the error on the evaluation of the weight of the zinc oxide nanowires in each investigated sample.

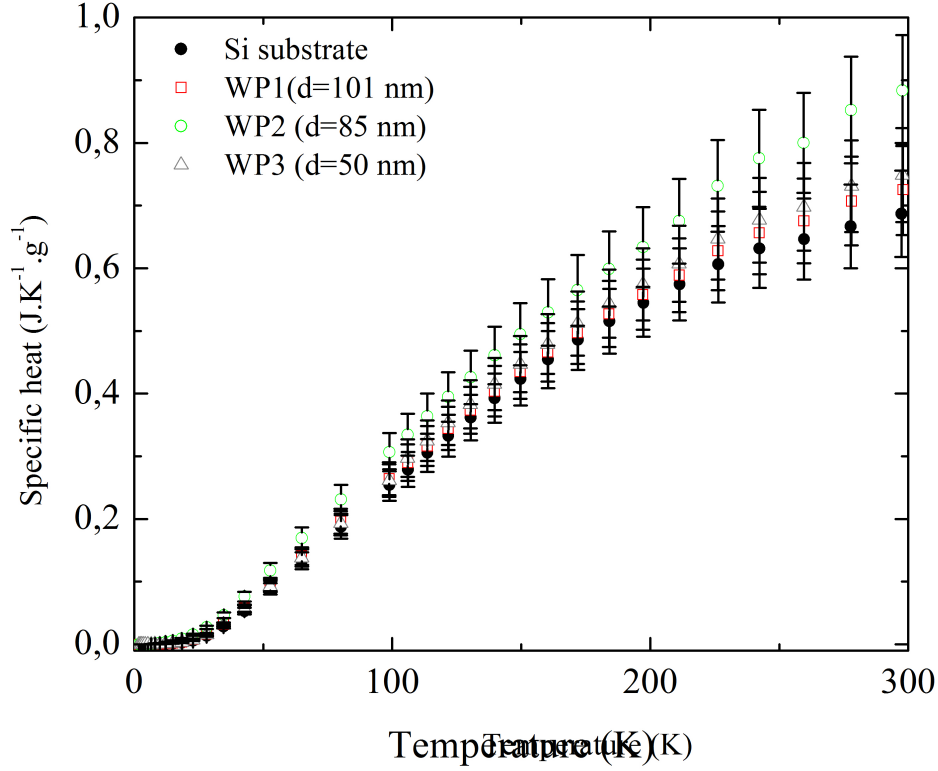


Figure 4.3: Specific heat of the Silicon substrate alone (open symbols) and of the substrate with nanowires (colored symbols)

The curves reveal a remarkable difference between the specific heat of the zinc oxide nanowires and that of the bulk Zinc Oxide beyond 25 K. This indicates an improvement of the specific heat at the nanometric scale compared to its bulk counterpart. Also this enhancement intensifies along the whole measured temperature range as the diameter of the Zinc Oxide nanowires increases.

As for the low temperature behavior, a bulk material's specific heat is usually governed by the following expression:

$$c = \gamma T + \beta T^3 \quad (4.1)$$

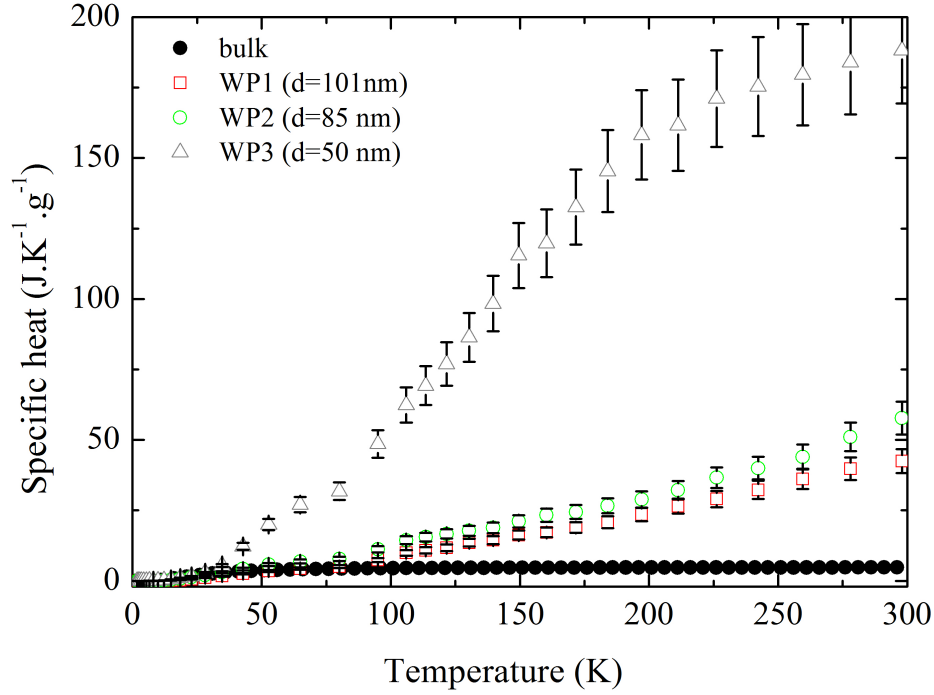


Figure 4.4: Specific heat of bulk ZnO obtained from first principles calculation (open symbols) and of the ZnO nanowires obtained from calorimetric measurements (colored symbols)

where the first term represents the contribution of the electron gas and the second term the contribution of the phonon harmonic dynamics to the total low-temperature specific heat. The common practice to separate out these two contributions is to first, divide the expression of c by T , then plot $\frac{c}{T}$ versus T^2 and finally find γ by extrapolating the curve to the ordinate axis and noting where it intersects.

To determine whether the Zinc Oxide nanowires' low temperature specific heat follows the typical three-dimensional T^3 behavior, we treat the nanowires specific heat curves in the same manner. Figure 4.5 shows the c/T curves for the Zinc Oxide nanowires and bulk ZnO.

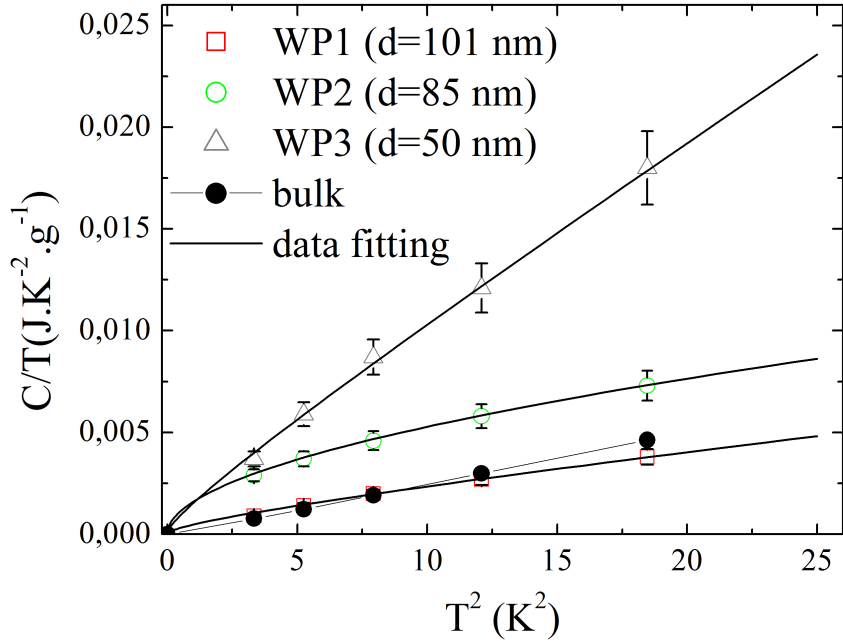


Figure 4.5: c/T versus T^2 for the Zinc Oxide bulk and nanowires. Open symbols correspond to data obtained from calorimetric measurements. Closed symbols correspond to data fitted with the model detailed in section 2.4

The curves indicate that the specific heat at low temperature is not a straight line proving that it deviates from the three-dimensional behavior. They also show that the deviation from the three-dimensional behavior increases as the diameter of the nanowires decreases.

A theoretical model has been developed for the purpose of explaining this deviation of the specific heat of nanowires from the T^3 behavior at low temperature. The model utilizes continuum mechanics with the proper boundary conditions to solve the equation of motion of a solid. The details of the model are developed in section 2.4. The theory results in the following form of the specific heat at low

temperatures;

$$c = \gamma T + 3pN_c k_B \times 7.212 \times \left(\frac{T}{\theta_{D,L}} \right)^2 + \frac{9}{2} pN_c k_B \times 25.980 \times \left(\frac{T}{\theta_{D,Q}} \right)^3 \quad (4.2)$$

where $\theta_{D,L}$ is the Debye temperature related to the phonons' mode of linear dispersion that gives rise to the contribution of the two-dimensional crystal, and $\theta_{D,Q}$ is the Debye temperature corresponding to the phonons' mode of quadratic dispersion that gives rise to contribution from three-dimensional crystal. Defining c/T we obtain:

$$c/T = \gamma + AT + BT^2 \quad (4.3)$$

with A being $3pN_c k_B \times 7.212 \times \frac{1}{\theta_{D,L}^2}$ and B equals to $\frac{9}{2} pN_c k_B \times 25.980 \times \frac{1}{\theta_{D,Q}^3}$. the c/T behavior clearly differs from that of a bulk material at low temperature by the contribution of T^2 . The specific heat of any solid at low temperature is characterized only by its Debye temperature. Equation 4.2 indicates that the low temperatures specific heat of any nanowire depends on the Debye temperatures of the two and three dimensional behavior. The model developed in section 2.4 for the specific heat gives theoretical expressions for $\theta_{D,L}$ and $\theta_{D,Q}$ and shows their dependence on the diameter and length of the nanowires. The theoretical curves for c/T are shown in figure 4.5 in solid lines. The best fit for the curves was obtained by neglecting the contribution from the electron gas and adjusting the values for $\theta_{D,L}$ and $\theta_{D,Q}$. The values that gave the best agreement are shown in table 4.1: The good agreement between the theoretical and experimental c/T values versus T^2 demonstrates that beside a contribution from a three-dimensional crystal, the nanowires' specific heat exhibits an appreciable contribution from a two-dimensional crystal.

Table 4.1: Debye temperatures of the ZnO nanowires in the measured samples.

Sample	$\theta_{D,L}$ (K)	$\theta_{D,Q}$ (K)
WP1(d=101 nm)	2200	330
WP2 (d=85 nm)	945	630
WP3 (d=50 nm)	1550	180

4.1.4 Graphene Measurement

The temperature response of clamped graphene was analyzed using the two-tau model. The results of the specific heat of the graphene measurements from 2.8 to 300 K are reported in figure 4.6. A comparison with experimental measurements of graphite obtained from ref. [5] is reported in figure 4.7.

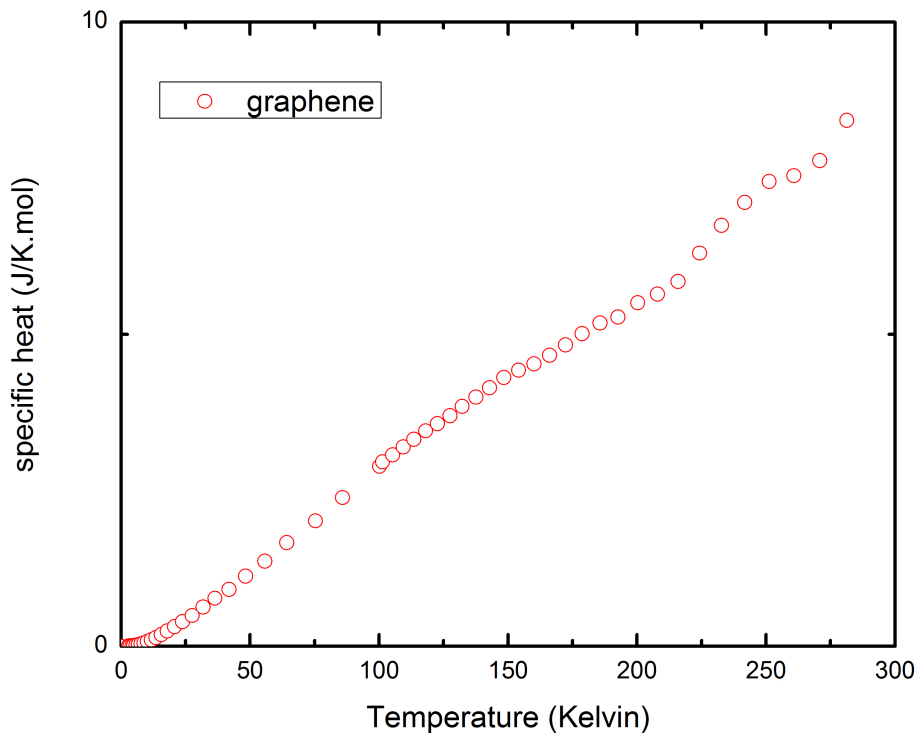


Figure 4.6: Specific heat of graphene reported from calorimetric measurements from 2.8 to 300 K

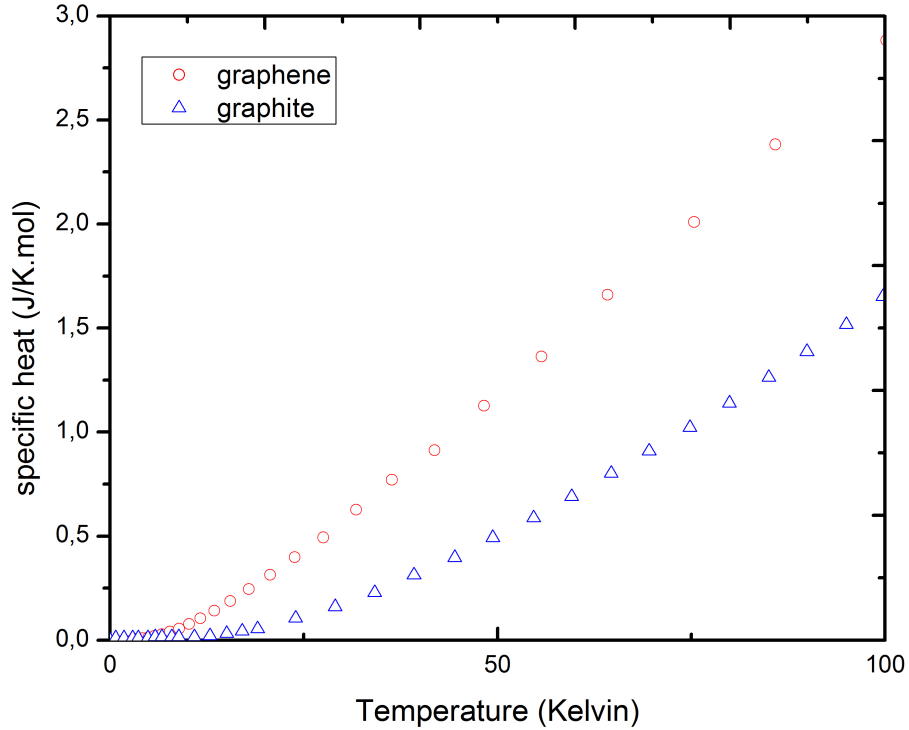


Figure 4.7: Specific heat of graphene reported from calorimetric measurements and experimental values of graphite adopted from [5]

The curves clearly indicate an enhancement in the experimental values of the specific heat of graphene in comparison to that of graphite. This fact is numerously mentioned in literature [5, 127–129]. Also, the enhancement factor of the specific heat of graphene compared to that of graphite increases as the temperature increases.

The low-temperatures behavior of clamped graphene is reported in figure 4.8. It shows that the c/T versus T curve corresponding to graphene is a straight line, indicating that the specific heat at low temperatures confirms the well reported theoretical T^2 dependence model for clamped graphene. The good agreement between the measured c/T versus T and the linear fit curve demonstrates that the

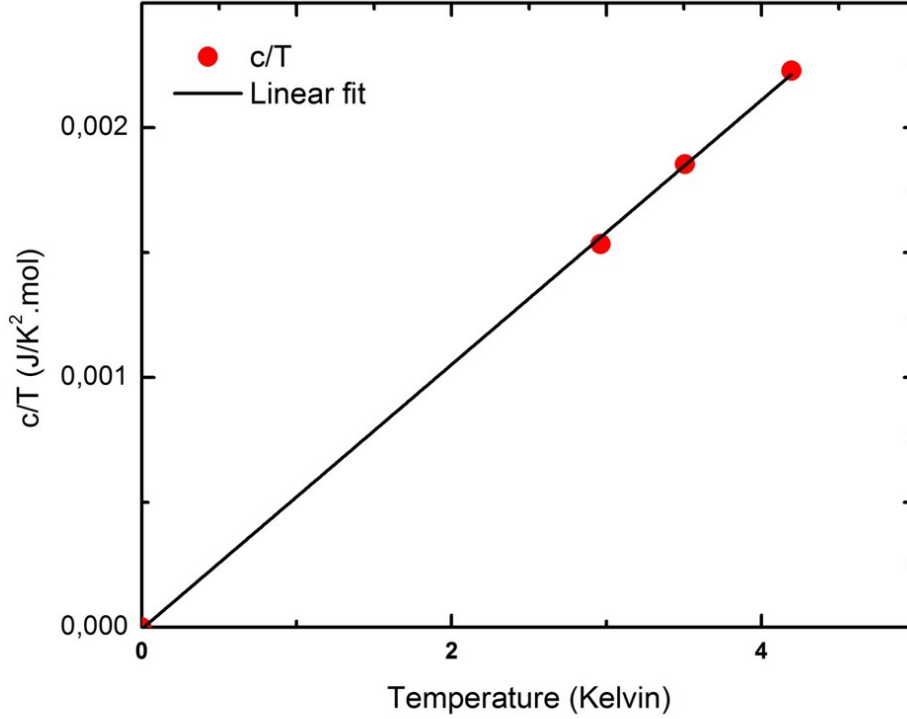


Figure 4.8: C/T vs T plot corresponding to the investigated graphene sample. closed symbols: Data obtained from calorimetric measurements. Solid Lines: Data obtained from linear fitting.

specific heat of graphene exhibits a contribution from a two-dimensional material as follows;

$$c/T = aT \Rightarrow c = aT^2 \quad (4.4)$$

Since the graphene sample is directly attached to the platform it is considered to be clamped. Therefore, the carbon atoms will not be able to move in the out of plane direction. This leads to the suppression of the out of plane mode. We speculate that the specific heat of graphene at low temperatures follows a two-dimensional behavior(T^2)as shown in figure 4.8 instead of linear T behavior reported in the theoretical models [5, 75, 87, 129] due to this suppression.

Also, a change in the slopes of the specific heat graph is noticed as the temperature increases. This indicates a probable "stairway" leap in the graphene's density of states with the change in frequency, which is confirmed by first principle calculations reported in ref. [101].

4.2 Thermal Conductance between Si substrate and ZnO nanowires

The data obtained from calorimetric measurements for the thermal conductance of the interface between Silicon and Zinc Oxide nanowires is plotted in figure 4.9. For comparison purposes, a theoretical study of the thermal conductance of the interface between Silicon and bulk Zinc Oxide was conducted using first principle calculations within the diffuse mismatch models [130]. The results are also plotted in figure 4.9. The figure shows that the thermal conductance of the Si/ZnO-nanowires interface is independent of the average size of the nanowires. Furthermore, the results indicate a noticeable difference in the thermal conductance of Si/ZnO-nanowires and the Si/bulk-ZnO, both in magnitude and temperature dependence. The thermal conductance of Si/ZnO-nanowires is lower than that of Si/bulk-ZnO by approximately five orders of magnitude. The reason why the thermal conductance value of Si/ZnO-nanowires is low in comparison to that of Si/bulk-ZnO may be attributed to the formation of a thin layer of low crystallinity at the interface between the ZnO nanowires and the Silicon substrate leading to a high rate phonon scattering. [131]. This result is supported by recent transmission electron microscopy, [132] which demonstrated that the thermal conductivity of phononic metamaterials is reduced mainly by phonon scattering in an intermixing region formed at the interface between the nanostructures and

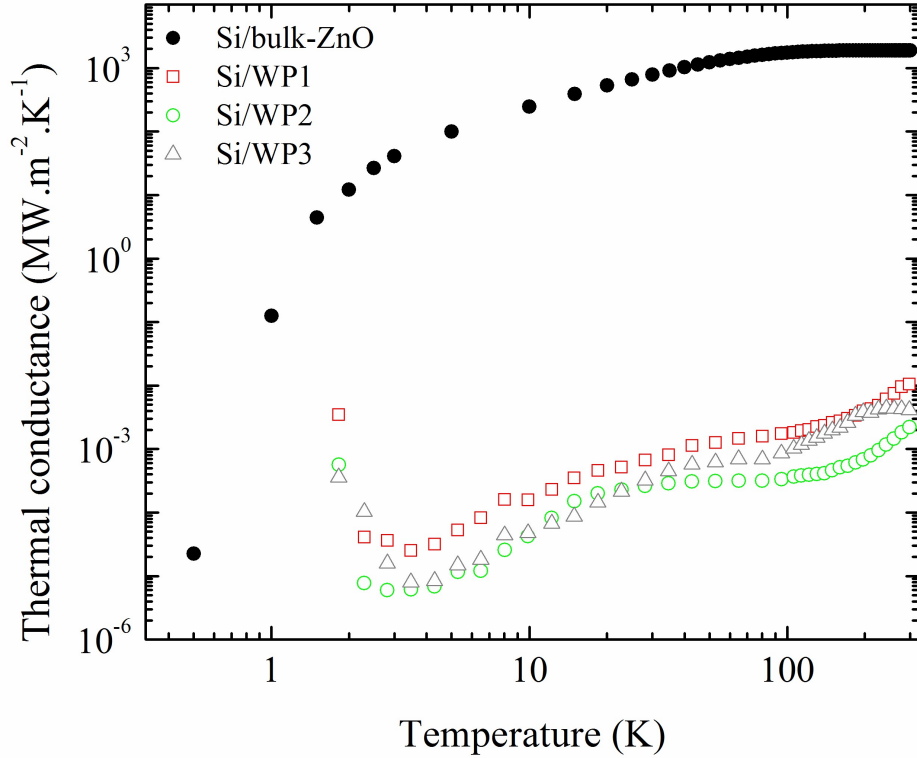


Figure 4.9: Thermal conductance of the interface between the Silicon substrate and the bulk ZnO obtained from first principles calculation (filled symbols) and of that between the substrate and ZnO nanowires obtained from calorimetric measurements (open symbols)

the underlying substrate.

Figure 4.9 also shows that the behavior of the thermal conductance of Si/ZnO-nanowires is highly temperature dependent; between 1.8 and 3 K, the thermal conductance drops rapidly, then it follows the behavior of the Si/bulk-ZnO curve from 3 to 70 K, and finally grows almost linearly at high temperatures. The rapid decrease between 1.8 and 3 K can be explained with the transition of phonon modes from specular to diffusive transmission as the temperature increases, or alternatively as the excited wavelength change. This is supported by

measurements of reflection of heat pulses from free surface solids, which showed that the phonon transmission changes from specular to diffusive when phonons of frequencies greater than 100 GHz are excited at a few degrees kelvin. [133]. As for the near linear growth of the thermal conductance of Si/ZnO-nanowires above 70 K, it can be attributed to the significant contribution of anharmonic phonon processes (which is not taken into account the diffuse mismatch model) that allows transfer of energy across the interface between the Silicon substrate and the Zinc Oxide nanowires. This contribution of anharmonic processes to the interface thermal conductance and its near linear growth have been previously observed in cases of interfaces between materials with highly dissimilar phonon spectra. [134]. Therefore, the contribution of the anharmonic processes to the thermal conductance between the Silicon substrate and the Zinc Oxide nanowires can be related to the strong mismatch between the phonon spectrum of the Zinc oxide nanowires and that of the Silicon substrate. As the temperature increases, the phonon anharmonic processes are enhanced, leading to an excess conductance at the interface between Si/ZnO-nanowires, which is revealed in the linear temperature dependence of the interface thermal conductance above 70 K.

Chapter 5

Conclusion

Heat pulse calorimetry was performed on Zinc Oxide nanowires and graphene samples from 1.8 to 300 K. The temperature response was analyzed using linear least square fitting methods to determine the specific heat of the nanowires and graphene and the thermal conductance of the interface between the nanowires and the underlying Silicon substrate. It is found that above 25 K, The specific heat of the nanowires is enhanced compared to that of the bulk Zinc Oxide and this enhancement increases as the temperature increases and the nanowires diameter decreases. As for the low temperatures behavior (below 4 K), the Zinc Oxide nanowires' specific heat was demonstrated to be essentially that of a two-dimensional crystal. The thermal conductance of the interface between the Silicon substrate and Zinc Oxide nanowires was found to be five orders of magnitude lower than that between bulk Zinc Oxide and Silicon substrate determined theoretically. This can be explained by the formation of thin layer of low crystallinity between the nanowires and Silicon substrate that increases the phonon scattering. A sharp drop in the thermal conductance between 1.8 and 3 K was attributed to the transition from specular to elastic diffusive transmission mode. The linear

increase above 70 k was interpreted also as a transition from diffusive elastic to diffusive inelastic transmission. The graphene's low temperature specific heat was found to follow a two-dimensional behavior. The two-dimensional trend of the specific heat of graphene at low-temperatures hence demonstrated an agreement with the T^2 dependence theory of the clamped graphene. At higher temperatures, this specific heat of graphene also showed an increase in its values in comparison with those of graphite.

As for the future of this work, an important exercise would be the investigation of the thermal properties of very thin nanowires at low-temperature to determine the discrepancy from the T^2+T^3 behavior. We speculate that very thin nanowires would admit a $T + T^2$ behavior due to the contribution of the one dimensionality of the wires.

Appendix A

Three-tau model derivation

The Balance Equations of the three-tau model are:

$$P(t) = c_1 \frac{dT_1}{dt} + \lambda_1(T_1 - T_0) + \lambda_2(T_1 - T_2) \quad (\text{A.1})$$

$$0 = c_2 \frac{dT_2}{dt} + \lambda_2(T_2 - T_1) + \lambda_3(T_2 - T_3) \quad (\text{A.2})$$

$$0 = c_3 \frac{dT_3}{dt} + \lambda_3(T_3 - T_2) \quad (\text{A.3})$$

Re-arranging the terms as function of Temperature;

$$P(t) = c_1 \frac{dT_1}{dt} + \lambda_1 T_1 - \lambda_1 T_0 + \lambda_2 T_1 - \lambda_2 T_2 \quad (\text{A.4})$$

$$0 = c_2 \frac{dT_2}{dt} + \lambda_2 T_2 - \lambda_2 T_1 + \lambda_3 T_2 - \lambda_3 T_3 \quad (\text{A.5})$$

$$0 = c_3 \frac{dT_3}{dt} + \lambda_3 T_3 - \lambda_3 T_2 \quad (\text{A.6})$$

$$P(t) = c_1 \frac{dT_1}{dt} + \lambda_1 T_1 - \lambda_1 T_0 + \lambda_2 T_1 - \lambda_2 T_2 \quad (\text{A.7})$$

$$0 = c_2 \frac{dT_2}{dt} + T_2(\lambda_2 + \lambda_3) - \lambda_2 T_1 + \lambda_3 T_2 \quad (\text{A.8})$$

$$0 = c_3 \frac{dT_3}{dt} + \lambda_3 T_3 - \lambda_3 T_2 \quad (\text{A.9})$$

Re-arranging the terms in equation A.1 as function of T_2 and deriving with respect to time we obtain:

$$\lambda_2 T_2 = c_1 \frac{dT_1}{dt} + \lambda_1 T_1 - \lambda_1 T_0 + \lambda_2 T_1 - P(t) \quad (\text{A.10})$$

$$\implies T_2 = \frac{1}{\lambda_2} [c_1 \frac{dT_1}{dt} + \lambda_1 T_1 - \lambda_1 T_0 + \lambda_2 T_1 - P(t)] \quad (\text{A.11})$$

$$\implies \frac{dT_2}{dt} = \frac{c_1}{\lambda_2} \frac{d^2 T_1}{dt^2} + \frac{\lambda_1}{\lambda_2} \frac{dT_1}{dt} + \frac{dT_1}{dt} - \frac{1}{\lambda_2} \frac{dP(t)}{dt} \quad (\text{A.12})$$

$$\implies \lambda_2 T_2 - \lambda_2 T_1 = c_1 \frac{dT_1}{dt} + \lambda_1 (T_1 - T_0) + \lambda_2 T_1 - P(t) \quad (\text{A.13})$$

$$\implies \lambda_2 (T_2 - T_1) = c_1 \frac{dT_1}{dt} + \lambda_1 (T_1 - T_0) - P(t) \quad (\text{A.14})$$

We now replace equations A.14 and A.16 in A.2 to eliminate T_2 :

$$0 = c_2 \left[\frac{c_1}{\lambda_2} \frac{d^2 T_1}{dt^2} + \frac{\lambda_1}{\lambda_2} \frac{dT_1}{dt} + \frac{dT_1}{dt} - \frac{1}{\lambda_2} \frac{dP(t)}{dt} \right] + [c_1 \frac{dT_1}{dt} + \lambda_1 (T_1 - T_0) - P(t)] + \lambda_3 (T_2 - T_3) \quad (\text{A.15})$$

$$0 = \frac{c_1 c_2}{\lambda_2} \frac{d^2 T_1}{dt^2} + \frac{\lambda_1 c_2}{\lambda_2} \frac{dT_1}{dt} + \frac{c_2 dT_1}{dt} - \frac{c_2}{\lambda_2} \frac{dP(t)}{dt} + c_1 \frac{dT_1}{dt} + \lambda_1 (T_1 - T_0) - P(t) + \lambda_3 (T_2 - T_3) \quad (\text{A.16})$$

Re-arranging the equation as function of T_3 and deriving with respect to time we obtain:

$$\implies 0 = \frac{c_1 c_2}{\lambda_2} \frac{d^2 T_1}{dt^2} + \frac{\lambda_1 c_2}{\lambda_2} \frac{dT_1}{dt} + \frac{c_2 dT_1}{dt} - \frac{c_2}{\lambda_2} \frac{dP(t)}{dt} + c_1 \frac{dT_1}{dt} + \lambda_1 (T_1 - T_0) - P(t) + \lambda_3 T_2 - \lambda_3 T_3 \quad (\text{A.17})$$

$$\begin{aligned} \implies \lambda_3 T_3 = & \frac{c_1 c_2}{\lambda_2} \frac{d^2 T_1}{dt^2} + \frac{\lambda_1 c_2}{\lambda_2} \frac{dT_1}{dt} + \frac{c_2 dT_1}{dt} \\ & - \frac{c_2}{\lambda_2} \frac{dP(t)}{dt} + c_1 \frac{dT_1}{dt} + \lambda_1 (T_1 - T_0) - P(t) + \lambda_3 T_2 \quad (\text{A.18}) \end{aligned}$$

$$\begin{aligned} T_3 = & \frac{1}{\lambda_3} \left[\frac{c_1 c_2}{\lambda_2} \frac{d^2 T_1}{dt^2} + \frac{\lambda_1 c_2}{\lambda_2} \frac{dT_1}{dt} + \frac{c_2 dT_1}{dt} \right. \\ & \left. - \frac{c_2}{\lambda_2} \frac{dP(t)}{dt} + c_1 \frac{dT_1}{dt} + \lambda_1 (T_1 - T_0) - P(t) + \lambda_3 T_2 \right] \quad (\text{A.19}) \end{aligned}$$

$$\begin{aligned} T_3 = & \frac{1}{\lambda_3} \left[\frac{c_1 c_2}{\lambda_2} \frac{d^2 T_1}{dt^2} + \left(\frac{\lambda_1 c_2}{\lambda_2} + c_2 + c_1 \right) \frac{dT_1}{dt} \right. \\ & \left. + \lambda_1 (T_1 - T_0) - \frac{c_2}{\lambda_2} \frac{dP(t)}{dt} - P(t) + \lambda_3 T_2 \right] \quad (\text{A.20}) \end{aligned}$$

$$\begin{aligned} \implies T_3 = & \frac{c_1 c_2}{\lambda_2 \lambda_3} \frac{d^2 T_1}{dt^2} + \frac{1}{\lambda_3} \left(\frac{\lambda_1 c_2}{\lambda_2} + c_2 + c_1 \right) \frac{dT_1}{dt} \\ & + \frac{\lambda_1}{\lambda_3} (T_1 - T_0) - \frac{c_2}{\lambda_3 \lambda_2} \frac{dP(t)}{dt} - \frac{1}{\lambda_3} P(t) + T_2 \quad (\text{A.21}) \end{aligned}$$

$$\begin{aligned} \implies \frac{dT_3}{dt} = & \frac{c_1 c_2}{\lambda_2 \lambda_3} \frac{d^3 T_1}{dt^3} + \left(\frac{\lambda_1 c_2}{\lambda_2 \lambda_3} + \frac{c_2}{\lambda_3} + \frac{c_1}{\lambda_3} \right) \frac{d^2 T_1}{dt^2} \\ & + \frac{\lambda_1}{\lambda_3} \frac{dT_1}{dt} - \frac{c_2}{\lambda_3 \lambda_2} \frac{d^2 P(t)}{dt^2} - \frac{1}{\lambda_3} \frac{dP(t)}{dt} + \frac{dT_2}{dt} \quad (\text{A.22}) \end{aligned}$$

We now replace A.14 in A.25

$$\begin{aligned} \implies \frac{dT_3}{dt} = & \frac{c_1 c_2}{\lambda_2 \lambda_3} \frac{d^3 T_1}{dt^3} + \left(\frac{\lambda_1 c_2}{\lambda_2 \lambda_3} + \frac{c_2}{\lambda_3} + \frac{c_1}{\lambda_3} \right) \frac{d^2 T_1}{dt^2} + \frac{\lambda_1}{\lambda_3} \frac{dT_1}{dt} - \frac{c_2}{\lambda_3 \lambda_2} \frac{d^2 P(t)}{dt^2} - \frac{1}{\lambda_3} \frac{dP(t)}{dt} \\ & + \left[\frac{c_1}{\lambda_2} \frac{d^2 T_1}{dt^2} + \frac{\lambda_1}{\lambda_2} \frac{dT_1}{dt} + \frac{dT_1}{dt} - \frac{1}{\lambda_2} \frac{dP(t)}{dt} \right] \quad (\text{A.23}) \end{aligned}$$

$$(T_3 - T_2) = \frac{c_1 c_2}{\lambda_2 \lambda_3} \frac{d^2 T_1}{dt^2} + \frac{1}{\lambda_3} \left(\frac{\lambda_1 c_2}{\lambda_2} + c_2 + c_1 \right) \frac{dT_1}{dt} + \frac{\lambda_1}{\lambda_3} (T_1 - T_0) - \frac{c_2}{\lambda_3 \lambda_2} \frac{dP(t)}{dt} - \frac{1}{\lambda_3} P(t) \quad (\text{A.24})$$

$$\lambda_3 (T_3 - T_2) = \frac{c_1 c_2}{\lambda_2} \frac{d^2 T_1}{dt^2} + \left(\frac{\lambda_1 c_2}{\lambda_2} + c_2 + c_1 \right) \frac{dT_1}{dt} + \lambda_1 (T_1 - T_0) - \frac{c_2}{\lambda_2} \frac{dP(t)}{dt} - P(t) \quad (\text{A.25})$$

We now replace equations A.27 and A.24 in A.3 to eliminate T_3 :

$$\begin{aligned} 0 = & c_3 \left[\frac{c_1 c_2}{\lambda_2 \lambda_3} \frac{d^3 T_1}{dt^3} + \left(\frac{\lambda_1 c_2}{\lambda_2 \lambda_3} + \frac{c_2}{\lambda_3} + \frac{c_1}{\lambda_3} \right) \frac{d^2 T_1}{dt^2} + \frac{\lambda_1}{\lambda_3} \frac{dT_1}{dt} - \frac{c_2}{\lambda_3 \lambda_2} \frac{d^2 P(t)}{dt^2} - \frac{1}{\lambda_3} \frac{dP(t)}{dt} \right. \\ & \left. + \left[\frac{c_1}{\lambda_2} \frac{d^2 T_1}{dt^2} + \frac{\lambda_1}{\lambda_2} \frac{dT_1}{dt} + \frac{dT_1}{dt} - \frac{1}{\lambda_2} \frac{dP(t)}{dt} \right] \right. \\ & \left. + \frac{c_1 c_2}{\lambda_2} \frac{d^2 T_1}{dt^2} + \left(\frac{\lambda_1 c_2}{\lambda_2} + c_2 + c_1 \right) \frac{dT_1}{dt} + \lambda_1 (T_1 - T_0) - \frac{c_2}{\lambda_2} \frac{dP(t)}{dt} - P(t) \right] \end{aligned} \quad (\text{A.26})$$

$$\begin{aligned} 0 = & \frac{c_1 c_2 c_3}{\lambda_2 \lambda_3} \frac{d^3 T_1}{dt^3} + \left(\frac{\lambda_1 c_2 c_3}{\lambda_2 \lambda_3} + \frac{c_2 c_3}{\lambda_3} + \frac{c_1 c_3}{\lambda_3} \right) \frac{d^2 T_1}{dt^2} + \frac{c_3 \lambda_1}{\lambda_3} \frac{dT_1}{dt} - \frac{c_2 c_3}{\lambda_3 \lambda_2} \frac{d^2 P(t)}{dt^2} - \frac{c_3}{\lambda_3} \frac{dP(t)}{dt} \\ & + \frac{c_1 c_3}{\lambda_2} \frac{d^2 T_1}{dt^2} + \frac{\lambda_1 c_3}{\lambda_2} \frac{dT_1}{dt} + c_3 \frac{dT_1}{dt} - \frac{c_3}{\lambda_2} \frac{dP(t)}{dt} \\ & + \frac{c_1 c_2}{\lambda_2} \frac{d^2 T_1}{dt^2} + \left(\frac{\lambda_1 c_2}{\lambda_2} + c_2 + c_1 \right) \frac{dT_1}{dt} + \lambda_1 (T_1 - T_0) - \frac{c_2}{\lambda_2} \frac{dP(t)}{dt} - P(t) \end{aligned} \quad (\text{A.27})$$

$$\begin{aligned} 0 = & \left(\frac{c_1 c_2 c_3}{\lambda_2 \lambda_3} \right) \frac{d^3 T_1}{dt^3} + \frac{d^2 T_1}{dt^2} \left(\frac{\lambda_1 c_2 c_3}{\lambda_2 \lambda_3} + \frac{c_2 c_3}{\lambda_3} + \frac{c_1 c_3}{\lambda_3} + \frac{c_1 c_3}{\lambda_2} + \frac{c_1 c_2}{\lambda_2} \right) \\ & + \frac{dT_1}{dt} \left(\frac{c_3 \lambda_1}{\lambda_2} + c_3 + \frac{c_2 \lambda_1}{\lambda_2} + c_2 + c_1 \right) + \lambda_1 T_1 \\ & - \frac{c_2 c_3}{\lambda_3 \lambda_2} \frac{d^2 P(t)}{dt^2} + \frac{dP(t)}{dt} \left(-\frac{c_2}{\lambda_2} - \frac{c_3}{\lambda_2} - \frac{c_3}{\lambda_3} \right) - \lambda_1 T_0 - P(t) \end{aligned} \quad (\text{A.28})$$

We omit the constant Temperature for its negligible contribution and we integrate with respect to time

$$\begin{aligned}
& \frac{c_1 c_2 c_3}{\lambda_2 \lambda_3} \frac{d^2 T_1}{dt^2} \Big|_0^t + \left(\frac{\lambda_1 c_2 c_3}{\lambda_2 \lambda_3} + \frac{c_2 c_3}{\lambda_3} + \frac{c_1 c_3}{\lambda_3} + \frac{c_1 c_3}{\lambda_2} + \frac{c_1 c_2}{\lambda_2} \right) \frac{dT_1}{dt} \Big|_0^t \\
& + \left(\frac{c_3 \lambda_1}{\lambda_2} + c_3 + \frac{c_2 \lambda_1}{\lambda_2} + c_2 + c_1 \right) T_1 \Big|_0^t + \lambda_1 \int_0^t T_1 dt \\
& = \frac{c_2 c_3}{\lambda_3 \lambda_2} \frac{dP(t)}{dt} \Big|_0^t + \left(\frac{c_2}{\lambda_2} + \frac{c_3}{\lambda_2} + \frac{c_3}{\lambda_3} \right) P(t) \Big|_0^t + \int_0^t P(t) dt \quad (\text{A.29})
\end{aligned}$$

we consider $\frac{d^2 T_1}{dt^2} \Big|_0^t = 0$ due to the negligible contribution of the second derivative.

We define the following variables;

$$V(t) = \frac{dT_1}{dt} \Big|_0^t \quad (\text{A.30})$$

$$H(t) = \frac{dP(t)}{dt} \Big|_0^t \quad (\text{A.31})$$

$$Q(t) = \int_0^t P(t) dt \quad (\text{A.32})$$

$$S(t) = \int_0^t T_1 dt \quad (\text{A.33})$$

$$\Gamma(t) = T_1 \Big|_0^t \quad (\text{A.34})$$

Replacing them in A.31 we obtain:

$$\begin{aligned}
& \left(\frac{\lambda_1 c_2 c_3}{\lambda_2 \lambda_3} + \frac{c_2 c_3}{\lambda_3} + \frac{c_1 c_3}{\lambda_3} + \frac{c_1 c_3}{\lambda_2} + \frac{c_1 c_2}{\lambda_2} \right) V(t) + \left(\frac{c_3 \lambda_1}{\lambda_2} + c_3 + \frac{c_2 \lambda_1}{\lambda_2} + c_2 + c_1 \right) \Gamma(t) \\
& + \lambda_1 S(t) = \frac{c_2 c_3}{\lambda_3 \lambda_2} H(t) + \left(\frac{c_2}{\lambda_2} + \frac{c_3}{\lambda_2} + \frac{c_3}{\lambda_3} \right) P(t) + Q(t) \quad (\text{A.35})
\end{aligned}$$

We define the coefficients of each variable:

$$v = \frac{\lambda_1 c_2 c_3}{\lambda_2 \lambda_3} + \frac{c_2 c_3}{\lambda_3} + \frac{c_1 c_3}{\lambda_3} + \frac{c_1 c_3}{\lambda_2} + \frac{c_1 c_2}{\lambda_2} \quad (\text{A.36})$$

$$= \frac{c_3}{\lambda_3} \frac{\lambda_1 c_2}{\lambda_2} + \frac{c_3}{\lambda_3} c_2 + \frac{c_3}{\lambda_3} c_1 + \frac{c_1}{\lambda_2} (c_3 + c_2)$$

$$g = \frac{c_3 \lambda_1}{\lambda_2} + c_3 + \frac{c_2 \lambda_1}{\lambda_2} + c_2 + c_1 \quad (\text{A.37})$$

$$= \frac{\lambda_1}{\lambda_2} (c_3 + c_2) + (c_2 + c_1 + c_3)$$

$$h = \frac{c_2 c_3}{\lambda_3 \lambda_2} = \frac{c_3}{\lambda_3} \frac{c_2}{\lambda_2} \quad (\text{A.38})$$

$$p = \frac{c_2}{\lambda_2} + \frac{c_3}{\lambda_2} + \frac{c_3}{\lambda_3} = \frac{c_3}{\lambda_3} + \frac{1}{\lambda_2} (c_2 + c_3) \quad (\text{A.39})$$

$$\text{let } X = \frac{c_3}{\lambda_3}$$

$$v = X \frac{\lambda_1 c_2}{\lambda_2} + X c_2 + X c_1 + \frac{c_1}{\lambda_2} (c_3 + c_2) \quad (\text{A.40})$$

$$= X \left(\frac{c_2 \lambda_1}{\lambda_2} + c_2 + c_1 \right) + \frac{c_1}{\lambda_2} (c_3 + c_2)$$

$$g = \frac{\lambda_1}{\lambda_2} (c_3 + c_2) + (c_2 + c_1 + c_3) \text{ independent of } X \quad (\text{A.41})$$

$$h = X \frac{c_2}{\lambda_2} \quad (\text{A.42})$$

$$p = X + \frac{1}{\lambda_2} (c_2 + c_3) \quad (\text{A.43})$$

$$vV(t) + g\Gamma(t) + \lambda_1 S(t) = hH(t) + pP(t) + Q(t) \quad (\text{A.44})$$

$$\boxed{\implies \Gamma(t) = \frac{1}{g} [hH(t) + pP(t) + Q(t) - vV(t) - \lambda_1 S(t)]}$$

$$(\text{A.45})$$

Bibliography

- [1] M. M. Rojo, O. C. Calero, A. Lopeandia, J. Rodriguez-Viejo, and M. Martín-Gonzalez, “Review on measurement techniques of transport properties of nanowires,” *Nanoscale*, vol. 5, no. 23, pp. 11526–11544, 2013.
- [2] G. Ventura and M. Perfetti, *Thermal properties of solids at room and cryogenic temperatures*. Springer, 2016.
- [3] “Quantum Design Physical Property Measurement System: Heat Capacity Option User’s Manual,” vol. 25th, no. 1085-150,.
- [4] R. Jehee, *The evolution of the ferromagnetic ordering of Co doped URhGe*.
- [5] D. L. Nika, A. I. Cocemasov, and A. A. Balandin, “Specific heat of twisted bilayer graphene: Engineering phonons by atomic plane rotations,” *Applied Physics Letters*, vol. 105, no. 3, p. 031904, 2014.
- [6] M. M. Waldrop, “More than moore,” *Nature*, vol. 530, no. 7589, pp. 144–148, 2016.
- [7] D. G. Cahill, W. K. Ford, K. E. Goodson, G. D. Mahan, A. Majumdar, H. J. Maris, R. Merlin, and S. R. Phillpot, “Nanoscale thermal transport,” *Journal of applied physics*, vol. 93, no. 2, pp. 793–818, 2003.

- [8] R. Prasher, T. Tong, and A. Majumdar, “Approximate analytical models for phonon specific heat and ballistic thermal conductance of nanowires,” *Nano letters*, vol. 8, no. 1, pp. 99–103, 2008.
- [9] J. A. Pascual-Gutiérrez, J. Y. Murthy, and R. Viskanta, “Limits of size confinement in silicon thin films and wires,” *Journal of Applied Physics*, vol. 102, no. 3, p. 034315, 2007.
- [10] M.-J. Huang, T.-M. Chang, C.-K. Liu, and C.-K. Yu, “A theoretical study of the specific heat and debye temperature of low-dimensional materials,” *International Journal of Heat and Mass Transfer*, vol. 51, no. 17-18, pp. 4470–4479, 2008.
- [11] M. Kazan and P. Masri, “The contribution of surfaces and interfaces to the crystal thermal conductivity,” *Surface Science Reports*, vol. 69, no. 1, pp. 1–37, 2014.
- [12] B. He, T. J. Morrow, and C. D. Keating, “Nanowire sensors for multiplexed detection of biomolecules,” *Current opinion in chemical biology*, vol. 12, no. 5, pp. 522–528, 2008.
- [13] R. A. X. Duan, Y. Huang and C. M. Lieber, “Single-nanowire electrically driven lasers,” *Nature*, vol. 421, p. 241–245, 2003.
- [14] . . M. Gratzel, Nature 414, “Photoelectrochemical cells,” *Nature*, vol. 414, p. 338–344, 2001.
- [15] X. S. Y. M. Lin and M. S. Dresselhaus, “Theoretical investigation of thermoelectric transport properties of cylindrical bi nanowires,” *Phys. Rev. B*, vol. 62, no. 7, 2000.

- [16] A. Dworkin, D. Sasmor, and E. Vanartsdalen, “ T^{-2} dependence of the low temperature specific heat of boron nitride,” *The Journal of Chemical Physics*, vol. 21, no. 5, pp. 954–955, 1953.
- [17] M. L. C. S. G. L. A. Z. N. K. B. A. Mizel, L. X. Benedict and W. P. Beyermann, “Analysis of the low-temperature specific heat of multiwalled carbon nanotubes and carbon nanotube ropes,” *Physical Review B*, vol. 60, p. 3264, 1999.
- [18] W. Yi, L. Lu, Z. Dian-Lin, Z. Pan, and S. Xie, “Linear specific heat of carbon nanotubes,” *Physical Review B*, vol. 59, no. 14, p. R9015, 1999.
- [19] C. Zhi, Y. Bando, C. Tang, and D. Golberg, “Specific heat capacity and density of multi-walled boron nitride nanotubes by chemical vapor deposition,” *Solid State Communications*, vol. 151, no. 2, pp. 183–186, 2011.
- [20] C. Dames, B. Poudel, W. Wang, J. Huang, Z. Ren, Y. Sun, J. Oh, C. Opeil, M. Naughton, and G. Chen, “Low-dimensional phonon specific heat of titanium dioxide nanotubes,” *Applied Physics Letters*, vol. 87, no. 3, p. 031901, 2005.
- [21] Z.-Z. Lin, C.-L. Huang, Z. Huang, and W.-K. Zhen, “Surface/interface influence on specific heat capacity of solid, shell and core-shell nanoparticles,” *Applied Thermal Engineering*, vol. 127, pp. 884–888, 2017.
- [22] Y. Xiao, X. Yan, J. Cao, J. Ding, Y. Mao, and J. Xiang, “Specific heat and quantized thermal conductance of single-walled boron nitride nanotubes,” *physical Review B*, vol. 69, no. 20, p. 205415, 2004.

- [23] J. Zheng, M. C. Wingert, J. Moon, and R. Chen, “Simultaneous specific heat and thermal conductivity measurement of individual nanostructures,” *Semiconductor Science and Technology*, vol. 31, no. 8, p. 084005, 2016.
- [24] N. Pradhan, H. Duan, J. Liang, and G. Iannacchione, “Specific heat and thermal conductivity measurements for anisotropic and random macroscopic composites of cobalt nanowires,” *Nanotechnology*, vol. 19, no. 48, p. 485712, 2008.
- [25] J. S. Kurtz, R. R. Johnson, M. Tian, N. Kumar, Z. Ma, S. Xu, and M. H. Chan, “Specific heat of superconducting zn nanowires,” *Physical review letters*, vol. 98, no. 24, p. 247001, 2007.
- [26] D. Li, Y. Wu, P. Kim, L. Shi, P. Yang, and A. Majumdar, “Thermal conductivity of individual silicon nanowires,” *Applied Physics Letters*, vol. 83, no. 14, pp. 2934–2936, 2003.
- [27] D. Li, Y. Wu, R. Fan, P. Yang, and A. Majumdar, “Thermal conductivity of si/sige superlattice nanowires,” *Applied Physics Letters*, vol. 83, no. 15, pp. 3186–3188, 2003.
- [28] A. I. Boukai, Y. Bunimovich, J. Tahir-Kheli, J.-K. Yu, W. A. Goddard Iii, and J. R. Heath, “Silicon nanowires as efficient thermoelectric materials,” *Nature*, vol. 451, no. 7175, p. 168, 2008.
- [29] A. I. Hochbaum, R. Chen, R. D. Delgado, W. Liang, E. C. Garnett, M. Najarian, A. Majumdar, and P. Yang, “Enhanced thermoelectric performance of rough silicon nanowires,” *Nature*, vol. 451, no. 7175, p. 163, 2008.
- [30] X. Zhao and Y. Dan, “A silicon nanowire heater and thermometer,” *Applied Physics Letters*, vol. 111, no. 4, p. 043504, 2017.

- [31] J. Yang, Y. Yang, S. W. Waltermire, X. Wu, H. Zhang, T. Gutu, Y. Jiang, Y. Chen, A. A. Zinn, R. Prasher, *et al.*, “Enhanced and switchable nanoscale thermal conduction due to van der waals interfaces,” *Nature Nanotechnology*, vol. 7, no. 2, p. 91, 2012.
- [32] J.-U. Lee, D. Yoon, H. Kim, S. W. Lee, and H. Cheong, “Thermal conductivity of suspended pristine graphene measured by raman spectroscopy,” *Physical Review B*, vol. 83, no. 8, p. 081419, 2011.
- [33] J. H. Seol, I. Jo, A. L. Moore, L. Lindsay, Z. H. Aitken, M. T. Pettes, X. Li, Z. Yao, R. Huang, D. Broido, *et al.*, “Two-dimensional phonon transport in supported graphene,” *Science*, vol. 328, no. 5975, pp. 213–216, 2010.
- [34] G. Chen, “Ballistic-diffusive heat-conduction equations,” *Physical Review Letters*, vol. 86, no. 11, p. 2297, 2001.
- [35] F. Alvarez, D. Jou, and A. Sellitto, “Phonon hydrodynamics and phonon-boundary scattering in nanosystems,” *Journal of Applied Physics*, vol. 105, no. 1, p. 014317, 2009.
- [36] J. Chen, G. Zhang, and B. Li, “How to improve the accuracy of equilibrium molecular dynamics for computation of thermal conductivity?,” *Physics Letters A*, vol. 374, no. 23, pp. 2392–2396, 2010.
- [37] B.-Y. Cao and Y.-W. Li, “A uniform source-and-sink scheme for calculating thermal conductivity by nonequilibrium molecular dynamics,” *The Journal of chemical physics*, vol. 133, no. 2, p. 024106, 2010.
- [38] N. Yang, X. Ni, J.-W. Jiang, and B. Li, “How does folding modulate thermal conductivity of graphene?,” *Applied Physics Letters*, vol. 100, no. 9, p. 093107, 2012.

- [39] C.-W. Chang, D. Okawa, H. Garcia, A. Majumdar, and A. Zettl, “Breakdown of fourier’s law in nanotube thermal conductors,” *Physical review letters*, vol. 101, no. 7, p. 075903, 2008.
- [40] G. Zhang and B. Li, “Thermal conductivity of nanotubes revisited: Effects of chirality, isotope impurity, tube length, and temperature,” *The Journal of chemical physics*, vol. 123, no. 11, p. 114714, 2005.
- [41] C. T. Bui, R. Xie, M. Zheng, Q. Zhang, C. H. Sow, B. Li, and J. T. Thong, “Diameter-dependent thermal transport in individual zno nanowires and its correlation with surface coating and defects,” *Small*, vol. 8, no. 5, pp. 738–745, 2012.
- [42] N. Yang, G. Zhang, and B. Li, “Ultralow thermal conductivity of isotope-doped silicon nanowires,” *Nano letters*, vol. 8, no. 1, pp. 276–280, 2008.
- [43] M. Wang, N. Yang, and Z.-Y. Guo, “Non-fourier heat conductions in nanomaterials,” *Journal of Applied Physics*, vol. 110, no. 6, p. 064310, 2011.
- [44] J. Chen, G. Zhang, and B. Li, “Remarkable reduction of thermal conductivity in silicon nanotubes,” *Nano letters*, vol. 10, no. 10, pp. 3978–3983, 2010.
- [45] M. Upadhyaya and Z. Aksamija, “Nondiffusive lattice thermal transport in si-ge alloy nanowires,” *Physical Review B*, vol. 94, no. 17, p. 174303, 2016.
- [46] L. Zhu, B. Li, and W. Li, “Phonon transport in silicon nanowires: The reduced group velocity and surface-roughness scattering,” *Physical Review B*, vol. 94, no. 11, p. 115420, 2016.

- [47] D. Fan, H. Sigg, R. Spolenak, and Y. Ekinici, “Strain and thermal conductivity in ultrathin suspended silicon nanowires,” *Physical Review B*, vol. 96, no. 11, p. 115307, 2017.
- [48] K. Muttalib and S. Abhinav, “Suppressing phonon transport in nanowires: A simple model for phonon–surface-roughness interaction,” *Physical Review B*, vol. 96, no. 7, p. 075403, 2017.
- [49] T. Zhang, S.-l. Wu, R.-t. Zheng, and G.-a. Cheng, “Significant reduction of thermal conductivity in silicon nanowire arrays,” *Nanotechnology*, vol. 24, no. 50, p. 505718, 2013.
- [50] J. Xie, A. Frachioni, D. Williams, and B. White Jr, “Thermal conductivity of a zno nanowire/silica aerogel nanocomposite,” *Applied Physics Letters*, vol. 102, no. 19, p. 193101, 2013.
- [51] Y. Zhang, Y. Shi, L. Pu, J. Wang, L. Pan, and Y. Zheng, “Enhancement of thermoelectric figure-of-merit in laterally-coupled nanowire arrays,” *Physics Letters A*, vol. 375, no. 28-29, pp. 2728–2732, 2011.
- [52] T. Zhang, S. Wu, J. Xu, R. Zheng, and G. Cheng, “High thermoelectric figure-of-merits from large-area porous silicon nanowire arrays,” *Nano Energy*, vol. 13, pp. 433–441, 2015.
- [53] R. Anufriev, R. Yanagisawa, and M. Nomura, “Aluminium nanopillars reduce thermal conductivity of silicon nanobeams,” *Nanoscale*, vol. 9, no. 39, pp. 15083–15088, 2017.
- [54] R. R. Nair, P. Blake, A. N. Grigorenko, K. S. Novoselov, T. J. Booth, T. Stauber, N. M. Peres, and A. K. Geim, “Fine structure constant defines

- visual transparency of graphene,” *Science*, vol. 320, no. 5881, pp. 1308–1308, 2008.
- [55] K. F. Mak, J. Shan, and T. F. Heinz, “Seeing many-body effects in single- and few-layer graphene: observation of two-dimensional saddle-point excitons,” *Physical review letters*, vol. 106, no. 4, p. 046401, 2011.
- [56] K. I. Bolotin, K. Sikes, Z. Jiang, M. Klima, G. Fudenberg, J. Hone, P. Kim, and H. Stormer, “Ultrahigh electron mobility in suspended graphene,” *Solid State Communications*, vol. 146, no. 9-10, pp. 351–355, 2008.
- [57] X. Du, I. Skachko, A. Barker, and E. Y. Andrei, “Approaching ballistic transport in suspended graphene,” *Nature nanotechnology*, vol. 3, no. 8, p. 491, 2008.
- [58] C. Lee, X. Wei, J. W. Kysar, and J. Hone, “Measurement of the elastic properties and intrinsic strength of monolayer graphene,” *science*, vol. 321, no. 5887, pp. 385–388, 2008.
- [59] A. A. Balandin, S. Ghosh, W. Bao, I. Calizo, D. Teweldebrhan, F. Miao, and C. N. Lau, “Superior thermal conductivity of single-layer graphene,” *Nano letters*, vol. 8, no. 3, pp. 902–907, 2008.
- [60] A. A. Balandin, “Thermal properties of graphene and nanostructured carbon materials,” *Nature materials*, vol. 10, no. 8, p. 569, 2011.
- [61] Z. Yan, G. Liu, J. M. Khan, and A. A. Balandin, “Graphene quilts for thermal management of high-power gan transistors,” *Nature communications*, vol. 3, p. 827, 2012.

- [62] S. Gilje, S. Han, M. Wang, K. L. Wang, and R. B. Kaner, “A chemical route to graphene for device applications,” *Nano letters*, vol. 7, no. 11, pp. 3394–3398, 2007.
- [63] S. Ghosh, W. Bao, D. L. Nika, S. Subrina, E. P. Pokatilov, C. N. Lau, and A. A. Balandin, “Dimensional crossover of thermal transport in few-layer graphene,” *Nature materials*, vol. 9, no. 7, p. 555, 2010.
- [64] J. Renteria, S. Legedza, R. Salgado, M. Balandin, S. Ramirez, M. Saadah, F. Kargar, and A. Balandin, “Magnetically-functionalized self-aligning graphene fillers for high-efficiency thermal management applications,” *Materials & Design*, vol. 88, pp. 214–221, 2015.
- [65] K. M. Shahil and A. A. Balandin, “Graphene–multilayer graphene nanocomposites as highly efficient thermal interface materials,” *Nano letters*, vol. 12, no. 2, pp. 861–867, 2012.
- [66] K. M. Shahil and A. A. Balandin, “Thermal properties of graphene and multilayer graphene: Applications in thermal interface materials,” *Solid State Communications*, vol. 152, no. 15, pp. 1331–1340, 2012.
- [67] Q.-Y. Li, K. Xia, J. Zhang, Y. Zhang, Q. Li, K. Takahashi, and X. Zhang, “Measurement of specific heat and thermal conductivity of supported and suspended graphene by a comprehensive raman optothermal method,” *Nanoscale*, vol. 9, no. 30, pp. 10784–10793, 2017.
- [68] L. Wirtz and A. Rubio, “The phonon dispersion of graphite revisited,” *Solid State Communications*, vol. 131, no. 3-4, pp. 141–152, 2004.
- [69] V. Perebeinos and J. Tersoff, “Valence force model for phonons in graphene and carbon nanotubes,” *Physical Review B*, vol. 79, no. 24, p. 241409, 2009.

- [70] K. Michel and B. Verberck, “Theory of the evolution of phonon spectra and elastic constants from graphene to graphite,” *Physical Review B*, vol. 78, no. 8, p. 085424, 2008.
- [71] H. Wang, Y. Wang, X. Cao, M. Feng, and G. Lan, “Vibrational properties of graphene and graphene layers,” *Journal of Raman Spectroscopy*, vol. 40, no. 12, pp. 1791–1796, 2009.
- [72] Z. Aksamija and I. Knezevic, “Lattice thermal conductivity of graphene nanoribbons: Anisotropy and edge roughness scattering,” *Applied Physics Letters*, vol. 98, no. 14, p. 141919, 2011.
- [73] G. Sanders, A. Nugraha, K. Sato, J. Kim, J. Kono, R. Saito, and C. Stanton, “Theory of coherent phonons in carbon nanotubes and graphene nanoribbons,” *Journal of Physics: Condensed Matter*, vol. 25, no. 14, p. 144201, 2013.
- [74] A. I. Cocemasov, D. L. Nika, and A. A. Balandin, “Phonons in twisted bilayer graphene,” *Physical Review B*, vol. 88, no. 3, p. 035428, 2013.
- [75] A. I. Cocemasov, D. L. Nika, and A. A. Balandin, “Engineering of the thermodynamic properties of bilayer graphene by atomic plane rotations: the role of the out-of-plane phonons,” *Nanoscale*, vol. 7, no. 30, pp. 12851–12859, 2015.
- [76] L. Lindsay and D. Broido, “Optimized tersoff and brenner empirical potential parameters for lattice dynamics and phonon thermal transport in carbon nanotubes and graphene,” *Physical Review B*, vol. 81, no. 20, p. 205441, 2010.

- [77] L. Lindsay, D. Broido, and N. Mingo, “Flexural phonons and thermal transport in multilayer graphene and graphite,” *Physical Review B*, vol. 83, no. 23, p. 235428, 2011.
- [78] D. Singh, J. Y. Murthy, and T. S. Fisher, “Mechanism of thermal conductivity reduction in few-layer graphene,” *Journal of Applied Physics*, vol. 110, no. 4, p. 044317, 2011.
- [79] L. Lindsay, W. Li, J. Carrete, N. Mingo, D. Broido, and T. Reinecke, “Phonon thermal transport in strained and unstrained graphene from first principles,” *Physical Review B*, vol. 89, no. 15, p. 155426, 2014.
- [80] Q. Lu, W. Gao, and R. Huang, “Atomistic simulation and continuum modeling of graphene nanoribbons under uniaxial tension,” *Modelling and Simulation in Materials Science and Engineering*, vol. 19, no. 5, p. 054006, 2011.
- [81] G. Barbarino, C. Melis, and L. Colombo, “Effect of hydrogenation on graphene thermal transport,” *Carbon*, vol. 80, pp. 167–173, 2014.
- [82] K. R. Hahn, C. Melis, and L. Colombo, “Thermal transport in nanocrystalline graphene investigated by approach-to-equilibrium molecular dynamics simulations,” *Carbon*, vol. 96, pp. 429–438, 2016.
- [83] T. Nihira and T. Iwata, “Temperature dependence of lattice vibrations and analysis of the specific heat of graphite,” *Physical Review B*, vol. 68, no. 13, p. 134305, 2003.
- [84] S. Kitipornchai, X. He, and K. Liew, “Continuum model for the vibration of multilayered graphene sheets,” *Physical Review B*, vol. 72, no. 7, p. 075443, 2005.

- [85] J. Qian, M. J. Allen, Y. Yang, M. Dutta, and M. A. Stroscio, “Quantized long-wavelength optical phonon modes in graphene nanoribbon in the elastic continuum model,” *Superlattices and Microstructures*, vol. 46, no. 6, pp. 881–888, 2009.
- [86] M. Droth and G. Burkard, “Acoustic phonons and spin relaxation in graphene nanoribbons,” *Physical Review B*, vol. 84, no. 15, p. 155404, 2011.
- [87] A. Alofi and G. Srivastava, “Phonon conductivity in graphene,” *Journal of Applied Physics*, vol. 112, no. 1, p. 013517, 2012.
- [88] A. Alofi and G. Srivastava, “Thermal conductivity of graphene and graphite,” *Physical Review B*, vol. 87, no. 11, p. 115421, 2013.
- [89] A. Alofi and G. Srivastava, “Evolution of thermal properties from graphene to graphite,” *Applied Physics Letters*, vol. 104, no. 3, p. 031903, 2014.
- [90] O. Dubay and G. Kresse, “Accurate density functional calculations for the phonon dispersion relations of graphite layer and carbon nanotubes,” *Physical Review B*, vol. 67, no. 3, p. 035401, 2003.
- [91] J. Maultzsch, S. Reich, C. Thomsen, H. Requardt, and P. Ordejón, “Phonon dispersion in graphite,” *Physical review letters*, vol. 92, no. 7, p. 075501, 2004.
- [92] N. Mounet and N. Marzari, “First-principles determination of the structural, vibrational and thermodynamic properties of diamond, graphite, and derivatives,” *Physical Review B*, vol. 71, no. 20, p. 205214, 2005.
- [93] M. Lazzeri, C. Attaccalite, L. Wirtz, and F. Mauri, “Impact of the electron-electron correlation on phonon dispersion: Failure of lda and gga dft

- functionals in graphene and graphite,” *Physical Review B*, vol. 78, no. 8, p. 081406, 2008.
- [94] J.-A. Yan, W. Ruan, and M. Chou, “Phonon dispersions and vibrational properties of monolayer, bilayer, and trilayer graphene: Density-functional perturbation theory,” *Physical review B*, vol. 77, no. 12, p. 125401, 2008.
- [95] R. Gillen, M. Mohr, C. Thomsen, and J. Maultzsch, “Vibrational properties of graphene nanoribbons by first-principles calculations,” *Physical Review B*, vol. 80, no. 15, p. 155418, 2009.
- [96] S. K. Gupta, H. R. Soni, and P. K. Jha, “Electronic and phonon bandstructures of pristine few layer and metal doped graphene using first principles calculations,” *AIP Advances*, vol. 3, no. 3, p. 032117, 2013.
- [97] L. Paulatto, F. Mauri, and M. Lazzeri, “Anharmonic properties from a generalized third-order ab initio approach: Theory and applications to graphite and graphene,” *Physical Review B*, vol. 87, no. 21, p. 214303, 2013.
- [98] T. Zhang, R. Heid, K.-P. Bohnen, P. Sheng, and C. T. Chan, “Phonon spectrum and electron-phonon coupling in zigzag graphene nanoribbons,” *Physical Review B*, vol. 89, no. 20, p. 205404, 2014.
- [99] J. Pešić, V. Damljanović, R. Gajić, K. Hingerl, and M. Belić, “Density functional theory study of phonons in graphene doped with li, ca and ba,” *EPL (Europhysics Letters)*, vol. 112, no. 6, p. 67006, 2016.
- [100] M. Mohr, J. Maultzsch, E. Dobardžić, S. Reich, I. Milošević, M. Damljanović, A. Bosak, M. Krisch, and C. Thomsen, “Phonon dispersion of graphite by inelastic x-ray scattering,” *Physical Review B*, vol. 76, no. 3, p. 035439, 2007.

- [101] F. D. Natterer, Y. Zhao, J. Wyrick, Y.-H. Chan, W.-Y. Ruan, M.-Y. Chou, K. Watanabe, T. Taniguchi, N. B. Zhitenev, and J. A. Stroscio, “Strong asymmetric charge carrier dependence in inelastic electron tunneling spectroscopy of graphene phonons,” *Physical review letters*, vol. 114, no. 24, p. 245502, 2015.
- [102] I. Calizo, A. Balandin, W. Bao, F. Miao, and C. Lau, “Temperature dependence of the raman spectra of graphene and graphene multilayers,” *Nano letters*, vol. 7, no. 9, pp. 2645–2649, 2007.
- [103] A. C. Ferrari, J. Meyer, V. Scardaci, C. Casiraghi, M. Lazzeri, F. Mauri, S. Piscanec, D. Jiang, K. Novoselov, S. Roth, *et al.*, “Raman spectrum of graphene and graphene layers,” *Physical review letters*, vol. 97, no. 18, p. 187401, 2006.
- [104] I. Calizo, W. Bao, F. Miao, C. N. Lau, and A. A. Balandin, “The effect of substrates on the raman spectrum of graphene: Graphene-on-sapphire and graphene-on-glass,” *Applied Physics Letters*, vol. 91, no. 20, p. 201904, 2007.
- [105] A. C. Ferrari, “Raman spectroscopy of graphene and graphite: disorder, electron–phonon coupling, doping and nonadiabatic effects,” *Solid state communications*, vol. 143, no. 1-2, pp. 47–57, 2007.
- [106] I. Calizo, I. Bejenari, M. Rahman, G. Liu, and A. A. Balandin, “Ultraviolet raman microscopy of single and multilayer graphene,” *Journal of Applied Physics*, vol. 106, no. 4, p. 043509, 2009.

- [107] K. Khanafer and K. Vafai, “Analysis of the anomalies in graphene thermal properties,” *International Journal of Heat and Mass Transfer*, vol. 104, pp. 328–336, 2017.
- [108] M. M. Sadeghi, M. T. Pettes, and L. Shi, “Thermal transport in graphene,” *Solid State Communications*, vol. 152, no. 15, pp. 1321–1330, 2012.
- [109] E. Pop, V. Varshney, and A. K. Roy, “Thermal properties of graphene: Fundamentals and applications,” *MRS bulletin*, vol. 37, no. 12, pp. 1273–1281, 2012.
- [110] M. Xia, Y. Song, and S. Zhang, “Specific heat of graphene nanoribbons,” *Physics Letters A*, vol. 375, no. 42, pp. 3726–3730, 2011.
- [111] A. Tari, *The specific heat of matter at low temperatures*. Imperial Coll., 2003.
- [112] J. Van Dam and O. Andersen, “Temperature dependence of the pd susceptibility,” *Solid State Communications*, vol. 14, no. 7, pp. 645–647, 1974.
- [113] W. Giaque, “Wf giaque and pf meads, j. am. chem. soc. 63, 1897 (1941),” *J. Am. Chem. Soc.*, vol. 63, p. 1897, 1941.
- [114] L. Boltzmann, *Vorlesungen über gasstheorie*, vol. 1. JA Barth, 1896.
- [115] D. Bloom, D. H. Lowndes Jr, and L. Finegold, “Low temperature specific heat of copper: Comparison of two samples of high purity,” *Review of Scientific Instruments*, vol. 41, no. 5, pp. 690–695, 1970.
- [116] A. Einstein, “Planck’s theory of radiation and the theory of specific heat,” *Ann. Phys*, vol. 22, pp. 180–190, 1907.

- [117] W. Ledermann, “A symptotic formulae relating to the physical theory of crystals,” *Proc. R. Soc. Lond. A*, vol. 182, no. 991, pp. 362–377, 1944.
- [118] P. F. Sullivan and G. Seidel, “Steady-state, ac-temperature calorimetry,” *Physical Review*, vol. 173, no. 3, p. 679, 1968.
- [119] R. Bachmann, F. DiSalvo Jr, T. Geballe, R. Greene, R. Howard, C. King, H. Kirsch, K. Lee, R. Schwall, H.-U. Thomas, *et al.*, “Heat capacity measurements on small samples at low temperatures,” *Review of Scientific Instruments*, vol. 43, no. 2, pp. 205–214, 1972.
- [120] B.-X. Wang, L.-P. Zhou, and X.-F. Peng, “Surface and size effects on the specific heat capacity of nanoparticles,” *International journal of thermophysics*, vol. 27, no. 1, pp. 139–151, 2006.
- [121] E. Lifshitz and L. Landau, *Theory of elasticity*. Pergamon Press, 1951.
- [122] D. L. Nika and A. A. Balandin, “Phonons and thermal transport in graphene and graphene-based materials,” *Reports on Progress in Physics*, vol. 80, no. 3, p. 036502, 2017.
- [123] J. P. Shepherd, “Analysis of the lumped τ^2 effect in relaxation calorimetry,” *Review of scientific instruments*, vol. 56, no. 2, pp. 273–277, 1985.
- [124] J. S. Hwang, K. J. Lin, and C. Tien, “Measurement of heat capacity by fitting the whole temperature response of a heat-pulse calorimeter,” *Review of Scientific Instruments*, vol. 68, no. 1, pp. 94–101, 1997.
- [125] “Precision and accuracy of the heat-pulse calorimetric technique: lowtemperature heat capacities of milligram-sized synthetic mineral samples,”

- [126] A. Gokarna, R. Parize, H. Kadiri, K. Nomenyo, G. Patriarche, P. Miska, and G. Lerondel, “Highly crystalline urchin-like structures made of ultrathin zinc oxide nanowires,” *RSC Advances*, vol. 4, no. 88, pp. 47234–47239, 2014.
- [127] C. P. Herrero and R. Ramírez, “Thermal properties of graphene from path-integral simulations,” *The Journal of Chemical Physics*, vol. 148, no. 10, p. 102302, 2018.
- [128] J. Hone, B. Batlogg, Z. Benes, A. Johnson, and J. Fischer, “Quantized phonon spectrum of single-wall carbon nanotubes,” *Science*, vol. 289, no. 5485, pp. 1730–1733, 2000.
- [129] V. N. Popov, “Low-temperature specific heat of nanotube systems,” *Physical Review B*, vol. 66, no. 15, p. 153408, 2002.
- [130] P. Reddy, K. Castelino, and A. Majumdar, “Diffuse mismatch model of thermal boundary conductance using exact phonon dispersion,” *Applied Physics Letters*, vol. 87, no. 21, p. 211908, 2005.
- [131] G. P. Srivastava, *The physics of phonons*. 1990.
- [132] R. Anufriev and M. Nomura, “Heat conduction engineering in pillar-based phononic crystals,” *Physical Review B*, vol. 95, no. 15, p. 155432, 2017.
- [133] e. b. A. C. A. W. Eisenmenger and J. P. Wolfe, *Phonon Scattering in Condensed Matter*. 1986.
- [134] H.-K. Lyo and D. G. Cahill, “Thermal conductance of interfaces between highly dissimilar materials,” *Physical Review B*, vol. 73, no. 14, p. 144301, 2006.